Collation of Fluctuating Buffet Pressures for the Mercury/Atlas and Apollo/Saturn Configurations

MCDONNELL

COLLATION OF FLUCTUATING BUFFET PRESSURES

FOR THE

MERCURY/ATLAS AND APOLLO/SATURN CONFIGURATIONS

by

J. D. Shelton

Prepared under Contract No. NAS 1-3179 by

MCDONNELL AIRCRAFT CORPORATION

St. Louis, Missouri

for

NATIONAL AERONAUTICS AND SPACE ADMINISTRATION

NASA CR-

COLLATION OF FLUCTUATING BUFFET PRESSURES

FOR THE MERCURY/ATLAS AND

APOLLO/SATURN CONFIGURATIONS

By J. D. Shelton

SUMMARY

17282

This report presents a collation of the root mean square fluctuating buffet pressures for the Mercury/Atlas and Apollo/Saturn configurations. Correlation of the data with Mach Number, streamwise location, and angle of attack is established. The results of the study indicate that the eventual description of a simple and realistic design criteria is possible. A method for arriving at such a criteria is proposed. Author

INTRODUCTION

One of the factors affecting the structural design of a vehicle is the fluctuating buffet pressures. Logically, the definition of all structural design loads is divided into three distinct parts.

1. Description of the input excitation to the vehicle.

2. Description of the vehicle transfer function relating the output to the input.

3. Description of the output response of the vehicle.

Normally, criteria are available for defining the level of the input for structural design loads. Currently, however, no such criteria exist for buffeting flows loads. As a result, the designer must rely upon past experience and expensive wind tunnel model testing in order to ensure adequate structural integrity for the vehicle. A method for defining the vehicles' transfer functions is described in detail in Reference (1). In order to effectively employ the method of analysis described in Reference (1), it is first necessary to have a realistic description of the input excitation. Ultimately it is desired to define the input excitation without the need of resorting to wind tunnel tests. The purpose of this paper can be stated as follows:

1. Correlate the rms fluctuating buffet pressures with Mach Number, streamwise location, and angle of attack.

2. Define other parameters which might offer a possible correlation to the buffeting pressures.

3. Propose a method which would lead to the eventual description of simple and realistic design criteria.

SYMBOLS

α	Angle of attack
d	Diameter
d( )	Derivative of quantity in parenthesis
ΔC_{Prms}	Root mean square pressure divided by free stream dynamic pressure
f	Frequency (cps)
L_D	Exponential decay function
M	Mach Number
n_i	Number of data points in band "i"
N_{tot}	Total number of data points in a sample
$N(\Delta C_P)$	Cumulative probability distribution of ΔC_{Prms}
ω	Frequency (rad/sec.)
Φ	Power spectral density
$p(\Delta C_{Prms})$	Probability density of ΔC_{Prms}
$P(\Delta C_{Prms})$	Probability distribution of ΔC_{Prms}
P_r	Reference pressure
$\bar{P}_{rms}$	Root mean square pressure
q_∞	Free stream dynamic pressure
S	Strouhal number ($\omega d/V$)
SPL	Sound pressure level (decibels)
σ	Root mean square value of a statistical sample
T	Transducer
U_c	Convection velocity
V	Free stream velocity
X	Distance in the streamwise direction

GENERAL DISCUSSION

Module/Missile configurations are characterized by conical and cylindrical shapes. Typical of the configurations are those of the Mercury/Atlas and Apollo/Saturn shown in Figure 1. The overall vehicle responds dynamically in the bending modes -- the mode shapes and frequencies being dependent upon the distribution of mass and stiffness, and, to a lesser extent, the damping. These modes are of primary concern for flutter analysis, gust analysis, transient maneuvers, etc.; and, in general, are centered in the lower end of the frequency spectrum. For the buffet and flows analysis the excitation and response are concerned with the modes associated with the local structure; e.g., the panels on the module or adapter. In general, these modal frequencies are in the central frequency spectrum; above this is the sonic excitation in the high frequency range.

For design purposes consideration must be given not only to each type of loading, but also, to the superposition of the various loadings; e.g., while the vehicle is maneuvering it could simultaneously encounter buffeting and atmospheric turbulence. Compared to the buffet analysis, methods for defining the excitation and response for most types of loadings are well defined. While buffet has been of some concern for design in the past, a method for realistically predicting the buffet loading in the early stages of design has become a necessity only recently. To this end numerous programs have been initiated to remedy the situation.

Currently, the method of analysis includes wind tunnel tests for a model of the configuration being studied. Pressure transducers are mounted on the model and time histories of the fluctuating pressure are measured. These time histories are then reduced to power spectral form where the spectral shapes and root mean square fluctuating pressures are defined. Similarly, the power spectral cross-correlation functions between the various transducer locations are defined. These then serve as the input excitation to the mathematical model representation of the elastic structure from which the root mean square structural output response may be defined. A representation for the description of the mathematical model of the elastic structure is given in Reference (1). The description of the input excitation, however, must still be obtained from wind tunnel tests.

The aerodynamics of the input excitation have received considerable attention in the past few years. It has been established that there are primarily three types of buffet -- boundary layer buffet, wake buffet, and buffet resulting from local characteristics such as an oscillating shock wave or detachment and re-attachment of the boundary layer. At any one point on the structure all three types can be acting simultaneously; and, in addition, each type of buffet can be the result of a combination of buffets generated at several different sources. From the studies of Coe for a flat plate in low speed subsonic flow it was determined that the boundary layer buffet dies out in a distance of 2-6 boundary layer thicknesses in the streamwise direction. This decay was well approximated by an exponential function. It was further determined that the convection velocity (U_c), i.e., the velocity at which the buffet flow travels up or downstream, is a function of the buffet flow frequency, and, to a lesser extent, the distance from the buffeting source.

It likewise appears reasonable to assume, at least qualitatively, that similar properties would exist for other types of buffet and at other Mach Numbers. Such properties, in fact, have been verified by other studies (Reference (2)). Intuitively, it is apparent that the random time history of pressure at a particular location on the body is the result of one or more random time histories generated at several different sources; e.g., the combination of the buffeting flows from the launch tower, boundary layer, local proturburences, oscillating shock waves, etc. It is thus readily apparent that the makeup of the buffeting flow is a complex aerodynamic phenomenon.

ANALYSIS OF FLUCTUATING BUFFET PRESSURE DATA

The fluctuating buffet pressure data utilized herein were obtained from the scale model wind tunnel tests of the Mercury/Atlas and Apollo/Saturn configurations. The four configurations considered are identified as follows:

1. MA-1: Mercury/Atlas exit configuration. (Launch tower off)
2. MA-2: Mercury/Atlas escape configuration. (Launch tower on)
3. Apollo C: Apollo/Saturn configuration without drag washer.
4. Apollo D: Apollo/Saturn configuration with drag washer.

The basic Mercury/Atlas and Apollo/Saturn configurations and their approximate pressure transducer locations are shown in Figure 1.

Root mean square (rms) fluctuating buffet pressure coefficients (ΔC_{Prms}) for the Mercury/Atlas configurations were taken from Reference (3). The ΔC_{Prms} values are listed in Table I for the various transducer locations, Mach Numbers, and angles of attack. Plots of sound pressure level (SPL) as a function of transducer location, Mach Number, and angle of attack are presented in Reference (4) for the Apollo/Saturn configurations. SPL values were converted to ΔC_{Prms} form in the following manner.

$$SPL = 10 \log_{10} \frac{\bar{P}_{rms}^2}{P_r^2}$$

where, P_r is the wind tunnel reference pressure level. ($P_r = 4.24 \times 10^{-7}$ psf) Thus,

$$\bar{P}_{rms} = P_r \sqrt{\text{anti-log}\left(\frac{SPL}{10}\right)}$$

and finally,

$$\Delta C_{Prms} = \frac{\bar{P}_{rms}}{q_\infty} = \frac{P_r}{q_\infty} \sqrt{\text{anti-log}\left(\frac{SPL}{10}\right)}$$

TABLE I

MERCURY/ATLAS FLUCTUATING BUFFET

PRESSURE COEFFICIENTS

Conf.	Transducer α	Transducer M	2 377	3 397	6 443	7 452	8 472	9 492	10 515	11 560	13 354	14 377
MA-1	+6	.90	.026	—	.076	.053	.051	.048	.011	.033	.034	.044
		1.00	.027	—	.071	.059	.052	.044	.012	.036	.105	.042
		1.20	.032	—	.062	.061	.035	.025	.013	.018	.095	.049
		1.40	.033	—	.064	.034	.029	.020	.016	.015	.082	.050
	+6	1.55	.041	—	.066	.025	.059	.028	.009	.016	.060	.037
	+3	.90	.026	—	.139	.068	.066	.065	.012	.044	.097	.039
		1.00	.027	—	.135	.062	.056	.058	.013	.045	.086	.039
		1.20	.028	—	.118	.045	.035	.026	.015	.020	.076	.039
		1.40	.026	—	.129	.034	.032	.039	.010	.016	.087	.039
		1.55	.044	—	.123	.028	.032	.030	.010	.018	.072	.031
	+3	1.63	.039	—	.114	.024	.031	.021	.006	.016	.059	.029
	0	.90	.126	—	.139	.101	.079	.083	.013	.061	.076	.039
		1.00	.025	—	.132	.072	.075	.076	.012	.054	.065	.037
		1.20	.025	—	.150	.034	.037	.032	.016	.016	.054	.033
		1.40	.025	—	.144	.030	.031	.020	.009	.015	.046	.029
		1.55	.042	—	.141	.023	.034	.019	.011	.015	.038	.026
	0	1.63	.036	—	.119	.018	.031	.017	.007	.015	.035	.023
	−3	.90	.045	—	.096	.073	.061	.076	.011	.066	.067	.034
		1.00	.027	—	.095	.064	.062	.074	.012	.056	.058	.032
		1.20	.021	—	.099	.027	.031	.028	.014	.014	.037	.031
		1.40	.023	—	.129	.026	.031	.016	.007	.014	.035	.026
		1.55	.042	—	.123	.022	.032	.017	.010	.014	.037	.025
	−3	1.63	.036	—	.117	.019	.031	.017	.006	.015	.039	.025
	−6	.90	.068	—	.093	.055	.056	.079	.012	.048	.088	.036
		1.00	.043	—	.098	.049	.060	.071	.012	.049	.067	.039
		1.20	.036	—	.123	.030	.035	.032	.017	.014	.031	.035
		1.40	.028	—	.120	.026	.029	.016	.007	.014	.039	.029
MA-1	−6	1.55	.042	—	.123	.023	.032	.017	.013	.014	.037	.028
MA-2	+6	.80	—	.042	.072	.059	.051	.046	.014	.023	.043	.051
		.90	—	.052	.075	.048	.048	.046	.008	.027	.042	.048
		.95	—	.042	.083	.049	.048	.047	.009	.030	.039	.048
		1.00	—	.042	.085	.047	.051	.047	.017	.033	.038	.046
		1.20	—	.042	.095	.041	.044	.028	.013	.019	.048	.033
	+6	1.40	.040	—	.131	.032	.042	.025	.005	.018	.040	.033
	+3	.80	—	.051	.110	.082	.069	.067	.025	.037	.040	.035
		.90	—	.065	.114	.066	.064	.064	.008	.039	.040	—
		.95	—	.049	.122	.069	.065	.062	.008	.043	.037	.034
		1.00	—	.051	.128	.073	.069	.063	.023	.043	.034	.033
		1.20	—	.046	.110	.033	.036	.026	.013	.017	.045	.029
	+3	1.40	.037	—	.139	.029	.036	.028	.005	.018	.032	.033
	0	.80	—	.069	.125	.106	.088	.091	.041	.053	.038	.029
		.90	—	.072	.138	.083	.081	.081	.008	.057	.040	.030
		.95	—	.060	.130	.093	.077	.076	.008	.060	.036	.027
		1.00	—	.060	.134	.085	.076	.079	.032	.053	.036	.029
		1.20	—	.052	.134	.030	.033	.025	.012	.014	.040	.028
	0	1.40	.037	—	.163	.026	.036	.031	.005	.015	.027	.033
	−3	.80	—	.080	.072	.075	.072	.085	.050	.061	.034	.024
		.90	—	.101	.089	.062	.064	.075	.008	.063	.034	.026
		.95	—	.067	.085	.064	.060	.070	.008	.064	.034	.025
		1.00	—	.067	.087	.068	.062	.071	.034	.055	.034	.024
		1.20	—	.056	.101	.025	.031	.022	.012	.013	.028	.025
	−3	1.40	.033	—	.127	.022	.031	.015	.005	.013	.022	.033
	−6	.80	—	—	.045	.050	.049	.069	.041	.037	.031	.024
		.90	—	.042	.052	.045	.044	.064	.008	.045	.032	.025
		.95	—	.095	.055	.042	.046	.067	.007	.049	.034	.025
		1.00	—	.087	.051	.045	.046	.059	.030	.047	.027	.024
		1.20	—	.073	.080	.022	.031	.021	.011	.011	.026	.026
MA-2	−6	1.40	.037	—	.110	.022	.031	.014	.005	.013	.018	.033

15 397	16 407	17 427	20 472	21 492	22 515	23 560	24 604	1C 472	4C 472	12C 472
.076	.115	.032	.074	.086	.123	.060	.024	.085	.060	.080
.073	.100	.043	.065	.017	.106	.063	.026	.084	.052	.081
.074	.077	.077	.031	.032	.020	.014	.012	.061	.018	.031
.092	.052	.053	.024	.011	.019	.010	.016	.038	.017	.025
.025	.042	.040	.020	.011	.014	.011	.010	.026	.021	.024
.071	.091	.061	.074	.083	.104	.062	.028	.077	.056	.083
.067	.078	.063	.075	.075	.091	.004	.030	.079	.059	.083
.065	.063	.108	.031	.032	.028	.017	.014	.036	.018	.034
.064	.058	.086	.027	.023	.025	.016	.014	.033	.018	.028
.075	.070	.080	.023	.010	.020	.014	.011	.026	.023	.029
.051	.056	.064	.023	.002	.019	.013	.011	.027	.021	.025
.056	.086	.055	.071	.073	.087	.060	.029	.085	.082	.083
.052	.059	.057	.073	.070	.080	.004	.032	.084	.061	.085
.048	.043	.088	.029	.032	.027	.018	.014	.036	.022	.029
.040	.031	.071	.027	.038	.024	.016	.014	.033	.018	.024
.058	.042	.072	.025	.016	.020	.003	.011	.026	.023	.026
.031	.033	.057	.023	.002	.019	.013	.012	.023	.026	.023
.042	.055	.044	.064	.064	.065	.047	.028	.088	.084	.083
.038	.037	.043	.062	.017	.063	.048	.028	.092	.061	.079
.035	.029	.064	.036	.024	.025	.018	.014	.034	.022	.037
.032	.026	.064	.027	.002	.024	.016	.012	.028	.018	.030
.035	.039	.067	.027	.002	.022	.005	.012	.021	.025	.032
.027	.031	.055	.025	.002	.021	.014	.012	.019	.026	.029
.042	.050	.034	.051	.039	.048	.034	.022	.077	.086	.076
.040	.034	.033	.055	.052	.049	.034	.024	.071	.061	.079
.031	.023	.044	.037	.024	.022	.016	.013	.025	.023	.040
.027	.022	.046	.021	.016	.017	.012	.010	.023	.018	.035
.030	.031	.051	.023	.002	.017	.013	.009	.019	.023	.035
.111	.081	.034	.050	.089	.174	.044	.019	.074	.069	.093
.078	.081	.038	.047	.075	.176	.050	.019	.075	.061	.091
.097	.078	.043	.045	.074	.006	.056	.020	.073	.060	.087
.096	.078	.039	.043	.069	.139	.056	.021	.068	.056	.087
.080	.091	.051	.017	.027	.030	.016	.013	.050	.025	.031
.078	.098	.039	.023	.015	.019	.015	.019	.026	.026	.024
.080	.065	.041	.052	.071	.133	.046	.021	.062	.091	.104
.059	.064	.045	.047	.068	.008	.053	.023	.062	.078	.098
.074	.062	.044	.045	.067	.136	.056	.023	.062	.073	.095
.071	.055	.042	.046	.062	.116	.053	.024	.060	.071	.093
.063	.077	.057	.021	.023	.036	.019	.015	.027	.024	.033
.065	.098	.049	.030	.030	.024	.018	.016	.023	.024	.024
.060	.061	.042	.050	.067	.005	.044	.024	.072	.074	.112
.052	.059	.045	.047	.065	.115	.006	.025	.075	.070	.104
.056	.057	.043	.045	.062	.112	.051	.027	.071	.069	.097
.056	.055	.039	.043	.058	.107	.049	.028	.072	.071	.100
.049	.055	.051	.022	.020	.036	.021	.015	.022	.029	.039
.056	.076	.046	.029	.034	.024	.018	.015	.019	.031	.034
.051	.052	.042	.046	.056	.005	.034	.019	.076	.066	.098
.046	.061	.043	.047	.059	.008	.039	.022	.078	.062	.094
.049	.050	.043	.043	.058	.097	.040	.021	.075	.059	.087
.049	.049	.041	.043	.058	.093	.041	.022	.076	.061	.091
.042	.043	.039	.021	.020	.035	.019	.013	.027	.022	.042
.040	.049	.034	.030	.021	.022	.017	.015	.024	.022	.036
—	.040	.038	.039	.044	.067	.027	.017	.052	.074	.081
.104	.042	.041	.040	.049	.008	.032	.019	.059	.068	.073
.044	.053	.043	.043	.053	.085	.035	.020	.060	.069	.069
.040	.040	.036	.041	.051	.081	.034	.021	.060	.071	.069
.042	.036	.031	.027	.027	.041	.020	.013	.091	.039	.049
.040	.046	.029	.028	.018	.019	.015	.012	.018	.034	.034

The resulting ΔC_{Prms} values for the Apollo/Saturn configurations are tabulated in Table II.

The variation of ΔC_{Prms} with Mach Number is shown in Figures 2 through 5. In general, ΔC_{Prms} tends to decrease with increasing M; however, it is noted that for some transducer locations ΔC_{Prms} increases with M while for others it is relatively insensitive to M. Figures 2 and 3, for the Mercury/Atlas configurations, show that the maximum values of ΔC_{Prms} occur in the vicinity of corners -- notably at transducer 6. In comparing the MA-1 and MA-2 data it is seen that the launch tower has no appreciable effect on the maximum levels of ΔC_{Prms}, however, the launch tower does tend to increase the general levels of ΔC_{Prms} for transonic Mach Numbers. Figures 4 and 5, for the Apollo/Saturn configurations, again show that the maximum values of ΔC_{Prms} occur in the vicinity of a corner -- transducer 2, 3, and 9. The values at .7M are unusually high -- this could be associated with subsonic flow characteristics. (If additional data were available in the range of M = .6 - .8 the results could be justified.) Comparison of Figures 4 and 5 show that the ΔC_{Prms} values for the Apollo D configuration are somewhat higher than those for the Apollo C. The difference is more pronounced for transonic Mach Numbers and is directly attributed to the presence of the drag washer on the Apollo D configuration.

To establish a correlation of ΔC_{Prms} with streamwise location the ΔC_{Prms} values were first normalized to one particular transducer location. For the MA-2 configuration, at zero degrees angle of attack, the ΔC_{Prms} values for a particular Mach Number were divided by the ΔC_{Prms} value at transducer 6. The resulting normalized coefficients are plotted in Figure 6 as a function of streamwise location for the various Mach Numbers. Forward of station 450 the effects of Mach Number are small, whereas aft of station 450 the data separates into a transonic group and a supersonic group. In comparing the "upper surface" to the "lower surface" there is little or no correlation -- this is at least partially explained by the antisymmetric shape of the Mercury capsule in the axial direction. For the Apollo D configuration, at zero degrees angle of attack, the ΔC_{Prms} values for a particular Mach Number were divided by 1.15 times the value at transducer 2 to arrive at a normalized value of 1.0. The resulting normalized coefficients are plotted in Figure 7 as a function of streamwise location for the various Mach Numbers. The curves for transonic Mach Numbers are insensitive to M forward of station 1770. Aft of station 1770, for $M \geq 1$, the curves are likewise insensitive to M; however, for $M < 1$ Mach Number does have an effect. The curves for supersonic Mach Numbers have a definite relationship to M. Forward of station 1770, the rate of increase of ΔC_{Prms} is more rapid for increasing M. Just aft of station 1770 there is a sharp "drop" in ΔC_{Prms}. The drop increases with increasing M suggesting that ΔC_{Prms} could be related to the static pressure distribution. After the initial drop in ΔC_{Prms} there is then a well defined decay with increasing streamwise distance. In an attempt to better define the decay of ΔC_{Prms} the preceding Apollo data were re-normalized to the value at transducer 3. These data are shown in Figure 8 in which x is measured positive aft of transducer 3. Empirical curves enveloping the data are shown on the figures. The empirical curves have an exponential decay from the initial value to a certain steady state value suggesting a decaying wake buffet leaving only the steady state boundary layer buffet. Subsonically, ΔC_{Prms} decays rather slowly, transonically the

TABLE II

APOLLO D FLUCTUATING BUFFET

PRESSURE COEFFICIENTS

Transducer											
α	M	1	2	3	4	5	6	7	8	9	10
0	.70	.165	—	.183	.116	—	—	—	—	.208	.122
	.89	.050	.106	.084	.045	.056	.054	.037	.031	.089	.047
	.92	.050	.106	.084	.043	.035	.027	.050	.037	.088	.046
	.96	.049	.106	.082	.041	.030	.022	.033	.033	.081	.043
	1.00	.046	.110	.097	.041	.029	.022	.030	.017	.097	.042
	1.06	.040	.103	.074	.039	.027	.021	.026	.017	.085	.044
	1.10	.049	.103	.074	.042	.029	.022	.023	.016	.048	.044
	1.20	.045	.104	.078	.080	.030	.021	.024	.017	.089	.040
	1.51	.042	.108	.070	.034	.023	.016	.017	.011	.072	.036
	1.76	.040	.103	.057	.032	—	—	.014	—	.061	.032
	2.00	.039	.105	.052	.030	—	—	.014	—	.057	.027
	2.49	.041	.112	.031	.020	—	—	—	—	.037	.020
	3.01	.045	.062	.020	—	—	—	—	—	.022	—
0	3.47	.063	.060	—	—	—	—	—	—	—	—
2	.70	—	—	.218	.092	—	—	—	—	.156	.16
	.89	.048	.106	.100	.056	.063	.054	.045	.035	.060	.03
	.92	.100	.112	.100	.060	.039	.030	.056	.043	.072	.03
	.96	.043	.101	.097	.053	.041	.027	.037	.036	.062	.03
	1.00	.046	.093	.077	.049	.033	.025	.033	.018	.066	.03
	1.06	.063	.082	.082	.044	.029	.022	.026	.018	.063	.03
	1.10	.043	.070	.088	.022	.030	.021	.026	.017	.070	.03
	1.20	.038	.078	.088	.040	.031	.021	.025	.019	.089	.04
	1.51	.041	.080	.070	.075	.024	.018	.018	.011	.075	.03
	1.76	.038	.081	.057	.032	—	—	.017	—	.062	.03
	2.00	.039	.087	.052	.031	—	—	—	—	.049	.03
	2.49	.039	.131	.037	.026	—	—	—	—	.027	.01
	3.01	.044	.110	.029	—	—	—	—	—	.019	—
2	3.47	.051	.133	—	—	—	—	—	—	—	—
4	.70	.165	—	.183	.069	—	—	—	—	.116	.15
	.89	.038	.084	.095	.067	.063	.048	.043	.035	.084	.02
	.92	.038	.082	.094	.065	.047	.035	.056	.043	.060	.02
	.96	.039	.077	.091	.062	.034	.027	.037	.039	.036	.02
	1.00	.040	.077	.091	.058	.029	.024	.033	.020	.040	.02
	1.06	.043	.074	.082	.058	.029	.021	.026	.018	.037	.02
	1.10	.041	.063	.088	.049	.033	.022	.022	.017	.047	.02
	1.20	.034	.068	.084	.042	.048	.021	.027	.019	.067	.03
	1.51	.045	.075	.061	.038	.025	—	.018	.013	.063	.03
	1.76	.040	.078	.051	.032	—	—	—	—	.048	.02
	2.00	.039	.087	.047	.031	—	—	—	—	.041	.02
	2.49	.035	.112	.031	.025	—	—	—	—	.026	.01
	3.01	.036	.093	.035	—	—	—	—	—	—	—
4	3.47	.047	.133	.032	—	—	—	—	—	—	—
6	.70	—	—	.173	.069	—	—	—	—	.097	.14
	.89	.044	.084	.089	.089	.063	.048	—	.037	.015	.01
	.92	.079	.084	.090	.076	.056	.043	.056	.047	.018	.01
	.96	.041	.082	.077	.069	.037	.035	.040	.039	.017	.01
	1.00	.046	.086	.054	.090	.031	.029	.030	.020	.017	.01
	1.06	.056	.078	.064	.062	.033	.022	.026	.019	.018	.01
	1.10	.044	.065	.074	.060	.033	.022	—	.018	.016	.0
	1.20	.048	.060	.081	.053	.034	.023	—	.019	.010	.01
	1.51	.047	.074	.058	.059	.029	.020	.020	.013	.045	.02
	1.76	.042	.074	.041	.036	—	—	—	—	.042	.02
	2.00	.040	.082	.042	.031	—	—	—	—	.036	.02
	2.49	.035	.101	.035	.022	—	—	—	—	.023	.01
	3.01	.037	.080	.035	—	—	—	—	—	.016	—
6	3.47	.047	.101	.029	—	—	—	—	—	—	—

	11	12	13									
	.097	—	.046									
	.060	.031	.040									
	.051	.027	.036									
	.047	.023	.031									
	.047	.020	—									
	.044	.019	—									
	.037	.018	—									
	.041	.029	—									
	.036	.011	.071									
	.034	—	.057									
	.035	—	.052									
	.031	—	.043									
	.031	—	.035									
	.027	—	.028									
5	.097	—	.032									
3	.069	—	.043									
3	.047	.071	.040									
3	.043	.041	.033									
5	.043	.023	—									
3	.044	.022	—									
5	.040	.019	—									
3	.045	.032	—									
7	.040	.012	.066									
2	.038	—	.057									
5	.038	—	.052									
5	.033	—	.046									
-	.033	—	.033									
-	.028	—	.028									
3	.104	—	.046									
4	.143	.031	.043									
2	.077	.027	.036									
1	.037	.024	.031									
2	.037	.022	—									
4	.040	.022	—									
5	.044	.021	—									
0	.053	.040	—									
0	.053	.013	.073									
5	.044	—	.061									
0	.040	—	.056									
2	.034	—	.048									
-	.034	—	.037									
-	.030	—	.030									
2	.109	—	.032									
5	.102	—	.046									
5	.034	.034	.042									
4	.029	.026	.035									
4	.029	.020	—									
4	.029	.019	—									
5	.031	.016	—									
3	.048	.038	—									
2	.080	.011	.064									
1	.050	—	.057									
9	.033	—	.056									
0	.026	—	.052									
1	.021	—	.038									
1	—	—	.031									

TABLE II (Concluded)

APOLLO D FLUCTUATING BUFFET

PRESSURE COEFFICIENTS

Transducer		1	2	3	4	5	6	7	8	9	10	11
α	M											
0	.70	—	—	.205	.061	.054	—	—	.049	.193	.069	.069
	.89	.053	.142	.127	.100	.064	—	.040	.031	.127	.089	.071
	.92	.063	.160	.124	.056	.079	.048	.047	.040	.127	.071	.066
	.96	.052	.140	.111	.055	.039	.042	.038	.035	.122	.055	.049
	1.00	.052	.149	.111	.055	.035	.025	.024	.022	.111	.056	.046
	1.06	.052	.143	.103	.052	.037	.026	.028	.021	.117	.056	.052
	1.10	.067	.143	.117	.058	.037	.026	.028	.021	.118	.065	.053
	1.20	.068	.142	.099	.051	.035	.026	.027	.021	.118	.063	.052
	1.51	.055	.114	.072	.042	.028	.021	.022	.013	.075	.047	.047
	1.76	.054	.120	.065	.038	.025	.018	.019	.011	.066	.038	.040
	2.00	.046	.138	.061	.034	.023	.015	.018	.011	.061	.047	.044
	2.49	.039	.155	.045	.027	.020	.013	.015	.010	.049	.029	.034
	3.01	.034	.168	.039	.025	.018	.011	.015	.010	.039	.018	.035
0	3.47	.038	.188	.035	.024	.015	.012	.015	.010	.042	.013	.033
2	.70	—	—	.210	.077	.077	—	—	.055	.218	—	—
	.89	.067	.180	.169	.112	.067	.056	.040	.046	.100	.056	.100
	.92	.112	.179	.159	.100	.064	.056	.067	.051	.112	.066	.095
	.96	.068	.161	.148	.078	.054	.049	.046	.051	.098	.054	.068
	1.00	.065	.161	.147	.077	.043	.036	.029	.031	.111	.058	.066
	1.06	.064	.142	.140	.065	.041	.030	.031	.026	.104	.060	.065
	1.10	.067	.120	.148	.062	.041	.030	.033	.026	.104	.062	.060
	1.20	.068	.116	.125	.063	.044	.032	.035	.025	.101	.063	.059
	1.51	.064	.113	.090	.059	.040	.028	.031	.019	.084	.053	.047
	1.76	.060	.116	.067	.051	.033	.025	.024	.016	.071	.051	.045
	2.00	.061	.107	.061	.047	.029	.022	.023	.015	.062	.055	.051
	2.49	.045	.089	.046	.034	.024	.016	.020	.012	.049	.030	.037
	3.01	.037	.074	.041	.026	.020	.014	.020	.012	.039	.026	.035
2	3.47	.040	.073	.037	.027	.021	.015	.022	.013	.032	.013	.035
4	.70	—	—	.153	.069	.065	—	—	.055	.154	.138	.092
	.89	.064	.126	.150	.103	.067	.064	.048	.047	.063	.035	.150
	.92	.069	.134	.159	.103	.064	.054	.062	.051	.071	.042	.112
	.96	.062	.112	.157	.071	.061	.043	.038	.045	.062	.036	.068
	1.00	.062	.112	.156	.070	.043	.035	.038	.030	.062	.036	.069
	1.06	.060	.107	.139	.065	.038	.028	.036	.025	.074	.041	.075
	1.10	.059	.086	.137	.065	.039	.028	.034	.024	.084	.049	.075
	1.20	.058	.082	.120	.062	.039	.030	.031	.023	.093	.051	.073
	1.51	.060	.067	.076	.057	.040	.029	.032	.019	.074	.047	.058
	1.76	.032	.064	.066	.056	.033	.026	.030	.017	.066	.045	.050
	2.00	.029	.067	.055	.042	.030	.023	.027	.016	.060	.052	.055
	2.49	.026	.073	.038	.031	.025	.018	.024	.015	.043	.030	.038
	3.01	.025	.090	.028	.029	.026	.016	.023	.015	.033	.016	.036
4	3.47	.030	.134	.035	.024	.021	.015	.022	.013	.025	.011	.035
6	.70	—	—	.139	.072	.081	—	—	.054	.109	—	—
	.89	.074	.100	.134	.104	.072	—	.040	.045	.028	.022	.150
	.92	.100	.112	.134	.089	.070	—	.071	.048	.035	.025	.085
	.96	.065	.092	.123	.072	.061	—	.048	.041	.035	.020	.062
	1.00	.063	.090	.123	.072	.050	.037	.045	.029	.062	.022	.062
	1.06	.061	.087	.126	.068	.043	.031	.040	.024	.037	.023	.065
	1.10	.062	.086	.130	.068	.046	.033	.039	.025	.048	.026	.066
	1.20	.061	.071	.114	.065	.046	.034	.035	.025	.058	.033	.079
	1.51	.060	.063	.066	.053	.041	.030	.030	.020	.059	.038	.066
	1.76	.050	.064	.055	.047	.033	.028	.024	.017	.064	.037	.050
	2.00	.043	.069	.043	.038	.031	.023	.023	.016	.052	.044	.058
	2.49	.035	.082	.031	.029	.025	.018	.022	.015	.035	.017	.034
	3.01	.031	.061	.028	.025	.022	.016	.023	.015	.026	.007	.033
6	3.47	.033	.053	.027	.024	.019	.015	.022	.013	.015	.009	.032

12	13									
—	.054									
.063	.035									
.047	.035									
.031	.033									
.022	—									
.021	—									
.021	—									
.020	—									
.013	—									
.010	—									
.009	—									
.007	.045									
.006	.037									
.006	.030									
—	.062									
.037	.022									
.079	.042									
.043	.035									
.043	—									
.037	—									
.033	—									
.032	—									
.014	—									
.012	—									
.011	—									
.009	.050									
.007	.040									
.007	.031									
—	.064									
.036	.041									
.048	.035									
.068	.034									
.036	—									
.037	—									
.029	—									
.026	—									
.020	—									
.016	—									
.013	—									
.010	.053									
.008	.045									
.009	.037									
—	.065									
.035	.045									
.038	.040									
.068	.035									
.026	—									
.028	—									
.023	—									
.023	—									
.014	—									
.012	—									
.011	—									
.009	.052									
.008	.043									
.009	.037									

decay is the most rapid, and supersonically, the decay rate decreases with increasing M. The steady state value of ΔC_{Prms} is the highest for subsonic M, lowest for transonic M, and then increases with Mach number for supersonic M.

The variation of ΔC_{Prms} with angle of attack is shown in Figures 9 and 10. Figure 9 is for transducer 6 on the MA-2 configuration. The shape of the curves are insensitive to M -- only the level is changed. The maximum ΔC_{Prms} values will occur for angles of attack near zero degrees. Figure 10 is for the Apollo D configuration. Since the Apollo D configuration is symmetrical in the axial direction, it is assumed that transducer 9 would represent negative angles of attack for transducer 3. The shapes of these curves again logically separate into subsonic, transonic, and supersonic groups. Transonically, the maximum ΔC_{Prms} values occur for an angle of attack between 2 and 4 degrees. Supersonically, the curves are symmetrical about 0 degrees angle of attack where the maximum ΔC_{Prms} values occur.

Power spectral densities of fluctuating buffet pressures at various transducer locations for the MA-2 configuration at M = 1 and $\alpha = +3°$ are shown in Figure 11. In general, these spectra could be fairly well approximated by "white noise" spectra. Frequency spectra of sound pressure levels at various transducer locations for the Apollo C and D configurations at M = 1 and $\alpha = 0°$ are shown in Figure 12. The maximum SPL for the C configuration occurs at a frequency that is about 20 percent higher than that for the D configuration. For a constant Strouhal number ($S = \omega d/V$) this is in accordance with the ratio of drag washer diameter (d_w) to escape tower base diameter (d_b); where, $d_w/d_b = 1.19$. The sound pressure level spectra for the D configuration are, in general, higher than those for the C configuration. For the Apollo D configuration, going in the streamwise direction from transducer 2 through transducers 3, 4, 5 and 8, it can be seen that the spectra are decaying at a more rapid rate for the frequencies below 150 cps.

A useful and an illuminating interpretation of the data is obtained by treating all of the data as a large statistical sample. For a normal or Gaussian distribution of a quantity the probability density is defined by:

$$p(\Delta C_{Prms}) = \frac{1}{\sigma}\sqrt{\frac{1}{2\pi}}\; e^{-\frac{\Delta C_{Prms}^2}{2\sigma^2}}$$

where, σ is the rms value of the statistical sample of ΔC_{Prms} values. Since only positive values of ΔC_{Prms} occur,

$$p(\Delta C_{Prms}) = \frac{1}{\sigma}\sqrt{\frac{2}{\pi}}\; e^{-\frac{\Delta C_{Prms}^2}{2\sigma^2}} \qquad \text{for } \Delta C_{Prms} \geq 0$$

$$p(\Delta C_{Prms}) = 0 \qquad \text{for } \Delta C_{Prms} < 0$$

The probability distribution is then defined as the integral of the probability density. Thus,

$$P(\Delta C_{Prms}) = \int p(\Delta C_{Prms})\, d(\Delta C_{Prms})$$

This equation cannot be integrated in closed form; however, between the limits of zero and infinity the value of the integral is 1.0. The Rayleigh probability density, which is related to the derivative of the normal probability density, is defined by:

$$p(\Delta C_{Prms}) = \frac{\Delta C_{Prms}}{\sigma^2} e^{-\frac{\Delta C_{Prms}^2}{2\sigma^2}} \qquad \text{for } \Delta C_{Prms} \geq 0$$

$$p(\Delta C_{Prms}) = 0 \qquad \text{for } \Delta C_{Prms} < 0$$

The probability that a certain value ΔC_{Prms} will not be exceeded is expressed by

$$P(\Delta C_{Prms}) = \int_0^{\Delta C_{Prms}} p(\Delta C_{Prms})\, d(\Delta C_{Prms}) = 1.0 - e^{-\frac{\Delta C_{Prms}^2}{2\sigma^2}}$$

Conversely, the probability of exceeding a certain value ΔC_{Prms}, i.e., the "cumulative" probability, is

$$N(\Delta C_{Prms}) = 1.0 - P(\Delta C_{Prms}) = e^{-\frac{\Delta C_{Prms}^2}{2\sigma^2}}$$

The fraction of ΔC_{Prms} values that fall in the interval between ΔC_{P1rms} and ΔC_{P2rms} ($\Delta C_{P2rms} > \Delta C_{P1rms}$) is then:

$$\frac{n_i}{N_{tot}} = N(\Delta C_{P1rms}) - N(\Delta C_{P2rms}) = e^{-\frac{\Delta C_{P1rms}^2}{2\sigma^2}} - e^{-\frac{\Delta C_{P2rms}^2}{2\sigma^2}}$$

In tabulating the data the number of ΔC_{Prms} values were counted for .01 bandwidths of ΔC_{Prms}, i.e., the number between 0 to .01 were counted, between .01 and .02, .02 and .03, etc. The resulting normalized values (n_i/N_{TOT}) are plotted in Figure 13 for all of the data and separately for the Mercury and Apollo data. Superimposed upon the figure are curves for the Rayleigh density for three different σ levels. The Rayleigh densities were obtained from the above equation for n_i/N_{TOT} and in reality should also be shown as steps; however, for the purpose of clarity they are shown as a smooth continuous curve. Figure 14 shows the density distributions for three different Mach Numbers. The "cumulative" probability distribution ($N(\Delta C_{Prms})$) is perhaps a simpler and clearer way to analyze the data. Cumulative probability distributions are

plotted against ΔC_{Prms} in Figure 15 for all of the data and separately for each configuration. For a single σ_2 level the curves should plot as a straight line, i.e., $-\log_e N(\Delta C_{Prms}) = \Delta C_{Prms}/2\sigma^2$, thus the rms value of the data (σ) may be defined by the slope $\left(\frac{1}{2\sigma^2}\right)$ of the curves. The curves of Figure 15 could be well approximated by one or more straight line curves -- this indicates one or more σ levels in the data. From the slope of the curves a maximum σ value of .06 is defined. At the 3σ level, this gives a ΔC_{Prms} of .18 which is in good agreement with the maximum value from the data. For a ΔC_{Prms} of .18 the maximum peak to peak fluctuating pressure on the body would then be approximately 0.46 q_∞ to 1.54 q_∞.

This approach to analyzing the data offers a variety of possibilities. For example, the data could be classified by Mach Number, Mach Number range (subsonic, transonic, and supersonic), angle of attack, profile surface shape (see sketch below), or any combination of these.

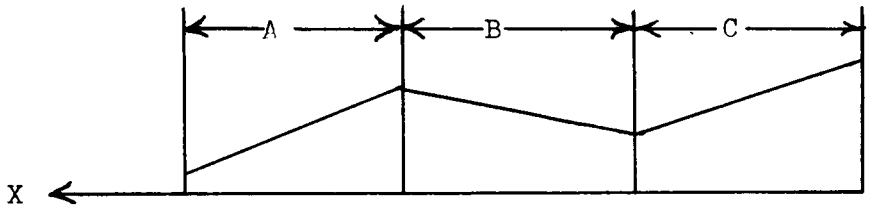

(For each of the surfaces A, B, and C there would be a different σ level for ΔC_{Prms}. For example, from the Mercury/Atlas data surface A generally has the highest ΔC_{Prms} values and surfaces B and C have somewhat lower values.) When data is gathered for additional configurations, it would appear to be logical to assign the data to general configuration classifications such as launch tower on or off, clean, dirty, etc. While a criteria cannot be defined based upon the results herein, the approach does offer promise as an aid in eventually defining a simple realistic design criteria.

CONCLUDING REMARKS

From the collation of the fluctuating buffet pressure data the following characteristics are noted.

(1) The fluctuating pressure level, $\Delta C_{P_{rms}}$, is related to Mach Number in a systematic fashion. In general, $\Delta C_{P_{rms}}$ is higher for transonic Mach Numbers than for supersonic Mach Numbers. Above transonic speeds $\Delta C_{P_{rms}}$ decreases with increasing M.

(2) The fluctuating pressure level, $\Delta C_{P_{rms}}$, is a function of streamwise locations. For the configurations studied the maximum $\Delta C_{P_{rms}}$ values generally occurred at the aft end of the first conical section -- transducer 6 for the Mercury/Atlas and transducer 2 for the Apollo/Saturn. Just aft of these points the percentage decrease in $\Delta C_{P_{rms}}$ increases with increasing Mach Number for $M > 1$. This suggests a possible correlation with the static pressure distribution. For the Apollo D configuration the $\Delta C_{P_{rms}}$ values aft of transducer 2 exhibit an exponential decay in the streamwise direction. A similar, although not as well defined, pattern is indicated for the Mercury/Atlas.

(3) The fluctuating pressure level, $\Delta C_{P_{rms}}$, is related to angle of attack. Generally, the maximum $\Delta C_{P_{rms}}$ values occur for angles of attack near zero degrees, and $\Delta C_{P_{rms}}$ is not overly sensitive to angle of attack.

(4) The Apollo/Saturn is a cleaner configuration than the Mercury/Atlas. While the maximum $\Delta C_{P_{rms}}$ values for the two are not significantly different, the general level of $\Delta C_{P_{rms}}$ is higher for the Mercury/Atlas. The buffet structure for the Apollo/Saturn is of a relatively simple form--composed of wake buffet shed from the launch escape system and a boundary layer buffet. Comparison of the Apollo C and D configurations indicates the influence of the launch escape system in generating a strong wake buffet. There is an indication that this buffet could be related to local drag characteristics of the launch escape system. The buffeting pressures for the Mercury/Atlas, on the other hand, are of an extremely complex form and appear to be the result of buffet generated at many different sources.

Collation of the fluctuating buffet pressures for a number of additional configurations offers promise in defining a preliminary form of design criteria. The required data should include the spectral densities, cross-spectral densities, and mean square values for the fluctuating buffet pressures at a number of locations on the body for Mach Numbers in the transonic and supersonic regimes. In this manner spectral shapes and root mean square values at the various locations can be empirically defined. Similarly, the time (or frequency) correlation between different locations can be defined. Because of the relatively low dynamic pressures, the fluctuating buffet pressures for subsonic speeds are probably of little concern for design purposes. Due to atmospheric turbulence, the angle of attack during launch cannot be realistically pre-defined, and indications are that is is of secondary importance; consequently, at the present, it should be disregarded as a parameter; logically, however, it should be verified that angle of attack is a secondary effect. From the collation of data a simple and yet reasonably realistic empirical design criteria could be defined. This criteria would involve:

(1) Define the magnitude and location of the maximum ΔC_{Prms} value on the body as a function of Mach Number and geometry.

(2) Relate streamwise and circumferential pressures to this reference value by means of the pertinent parameters including the appropriate decay functions.

(3) The spectral shape for the buffeting pressures initially could be assumed to be flat, i.e., white noise. As the "state of the art" advances the spectral shape can be defined as a function of Mach Number and geometry.

REFERENCES

1. Schweiker, J. W., and Davis, R. E., "Response of Complex Shell Structures to Aerodynamic Noise," (Proposed NASA CR).

2. Rainey, A. G., "Program on the Launch Vehicle Buffeting Problem," J. Spacecraft and Rockets, Volume 2, No. 3, May-June 1965.

3. Goldberg, A. P., and Adams, R. H., "Mercury-Atlas Buffeting Loads at Transonic and Low Supersonic Speeds," STL/TR-60-0000-AS431, November 1960.

4. Gildea, D. J., "Preliminary Report of Transient Pressures Measured on the 0.055 Scale Apollo Pressure Model (PSTL-1) in NAA Trisonic Wind Tunnel," SID62-1151, September 1962.

Mercury/Atlas

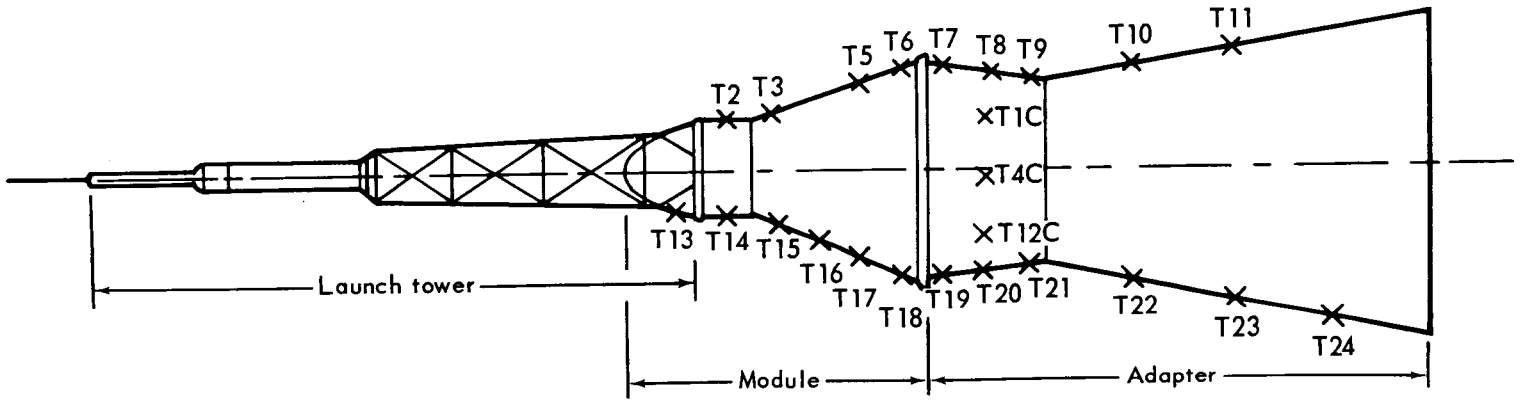

Apollo/Saturn

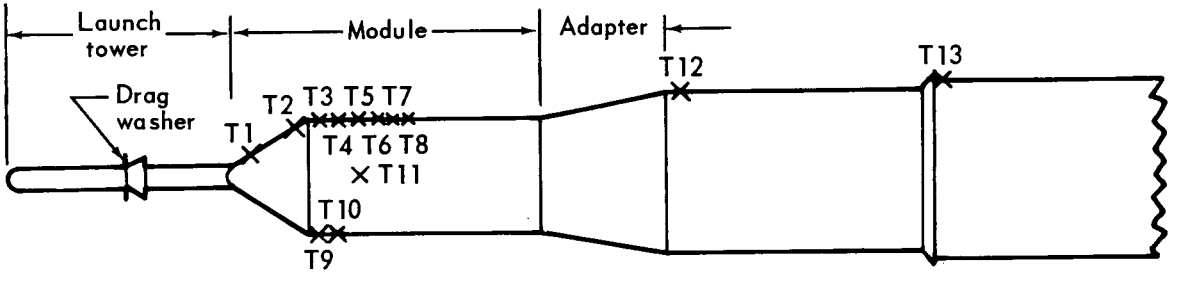

Figure 1 – Transducer Locations for the Mercury/Atlas and Apollo/Saturn Configurations

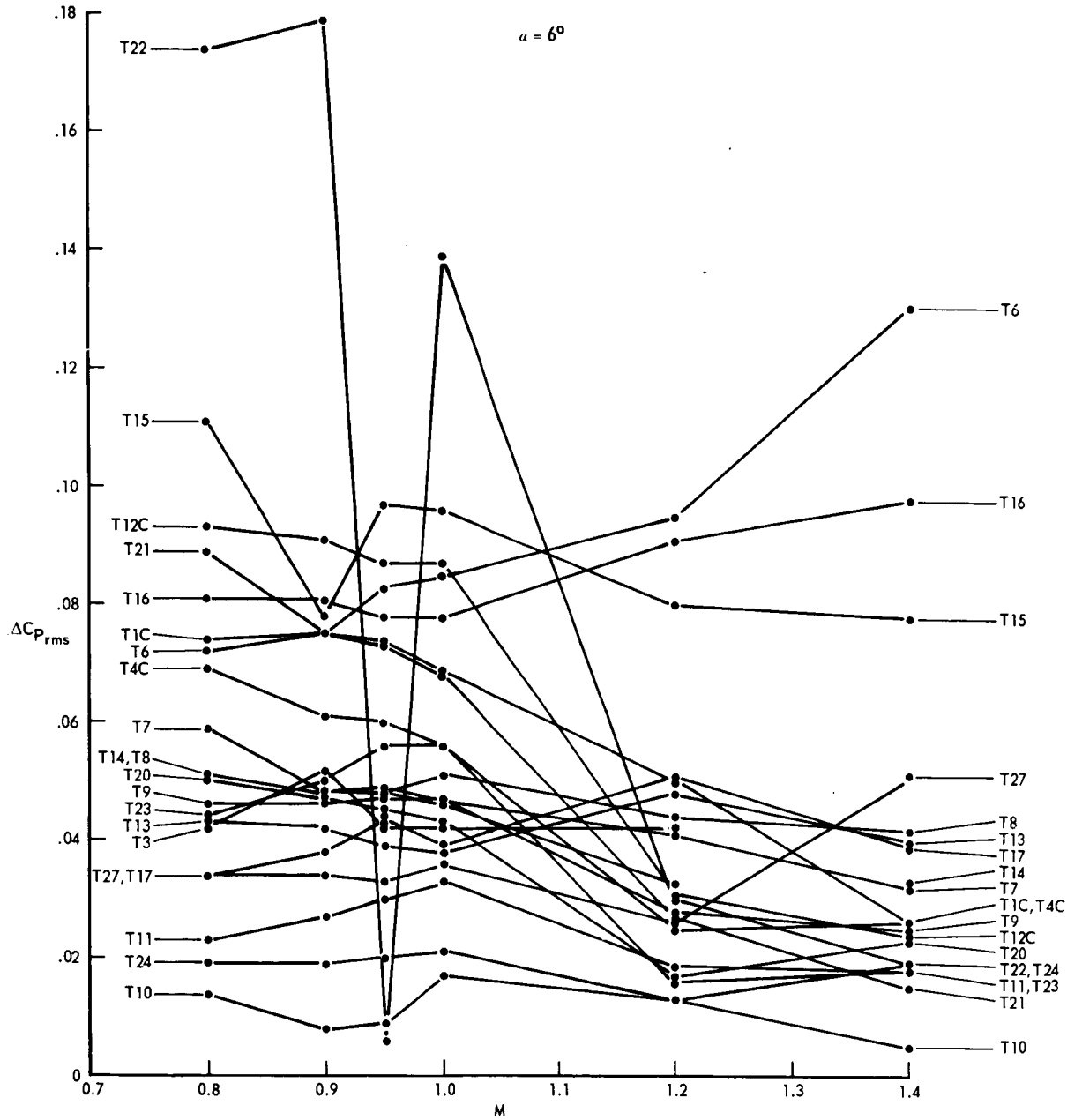

Figure 2 – Variation of Fluctuating Pressure Coefficients with Mach Number for Various Transducer Locations: MA–2

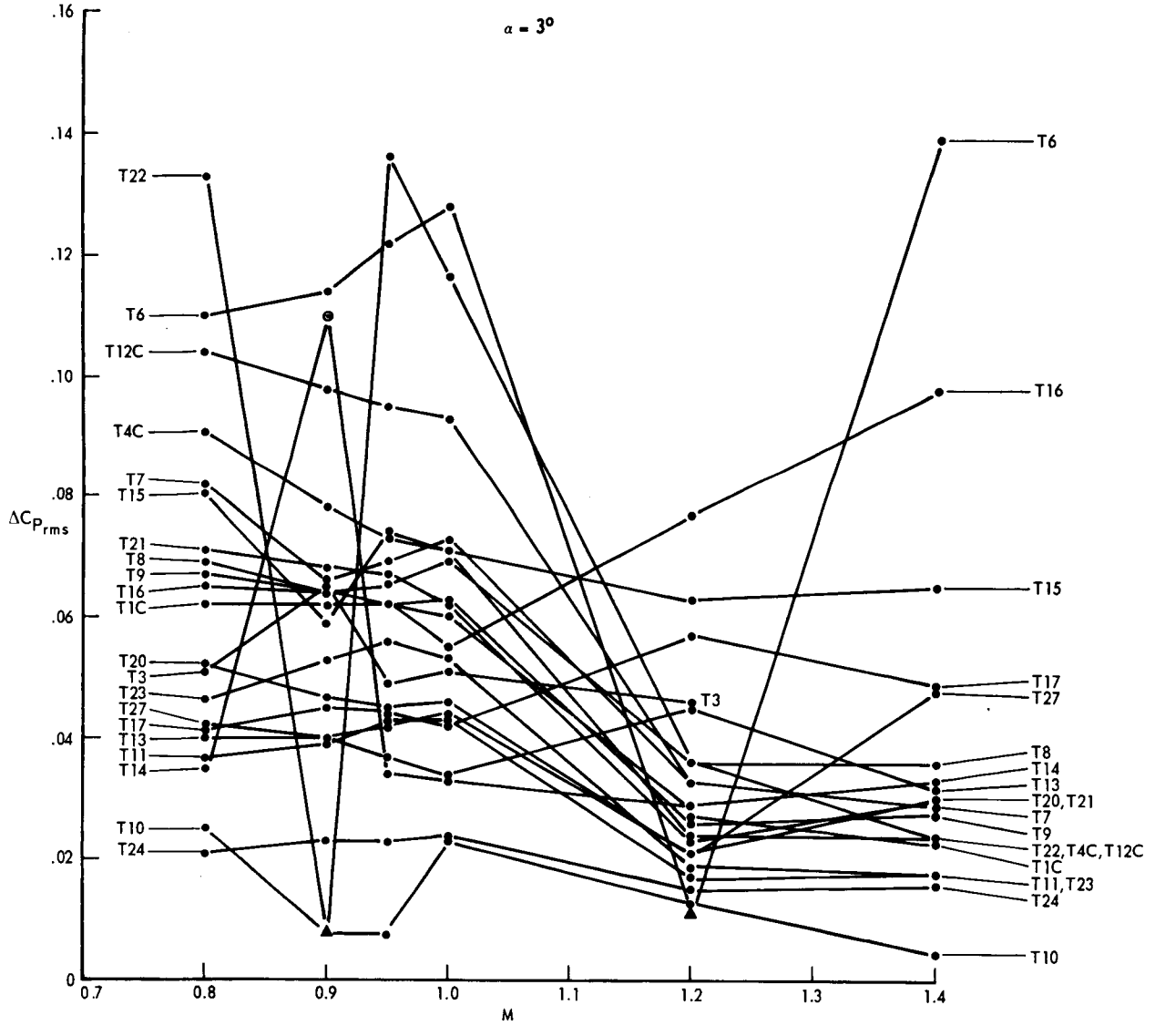

Figure 2 – Variation of Fluctuating Pressure Coefficients with Mach Number for Various Transducer Locations: MA–2 (Continued)

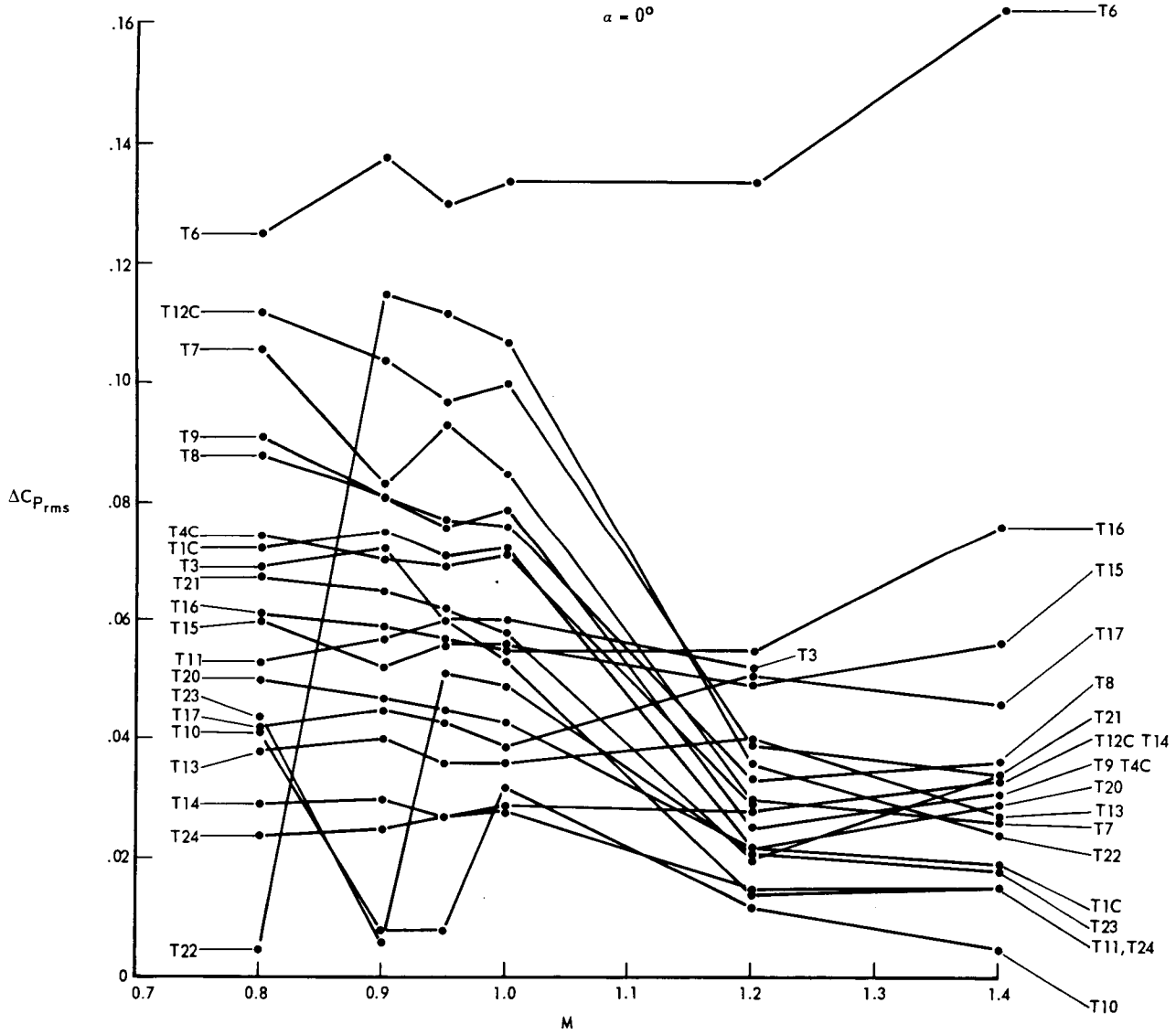

Figure 2 – Variation of Fluctuating Pressure Coefficients with Mach Number for Various Transducer Locations: MA–2 (Continued)

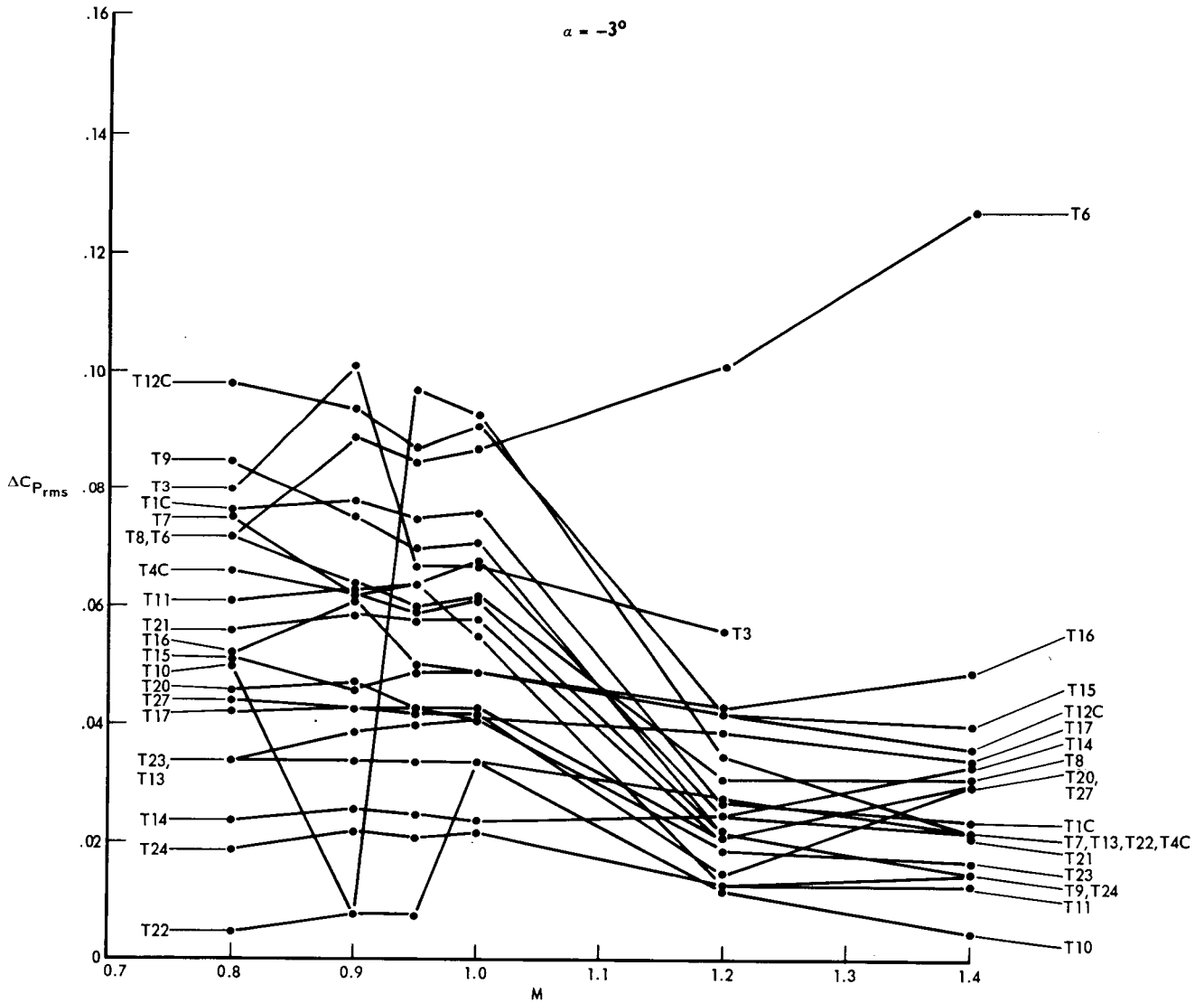

Figure 2 – Variation of Fluctuating Pressure Coefficients with Mach Number for Various Transducer Locations: MA–2 (Continued)

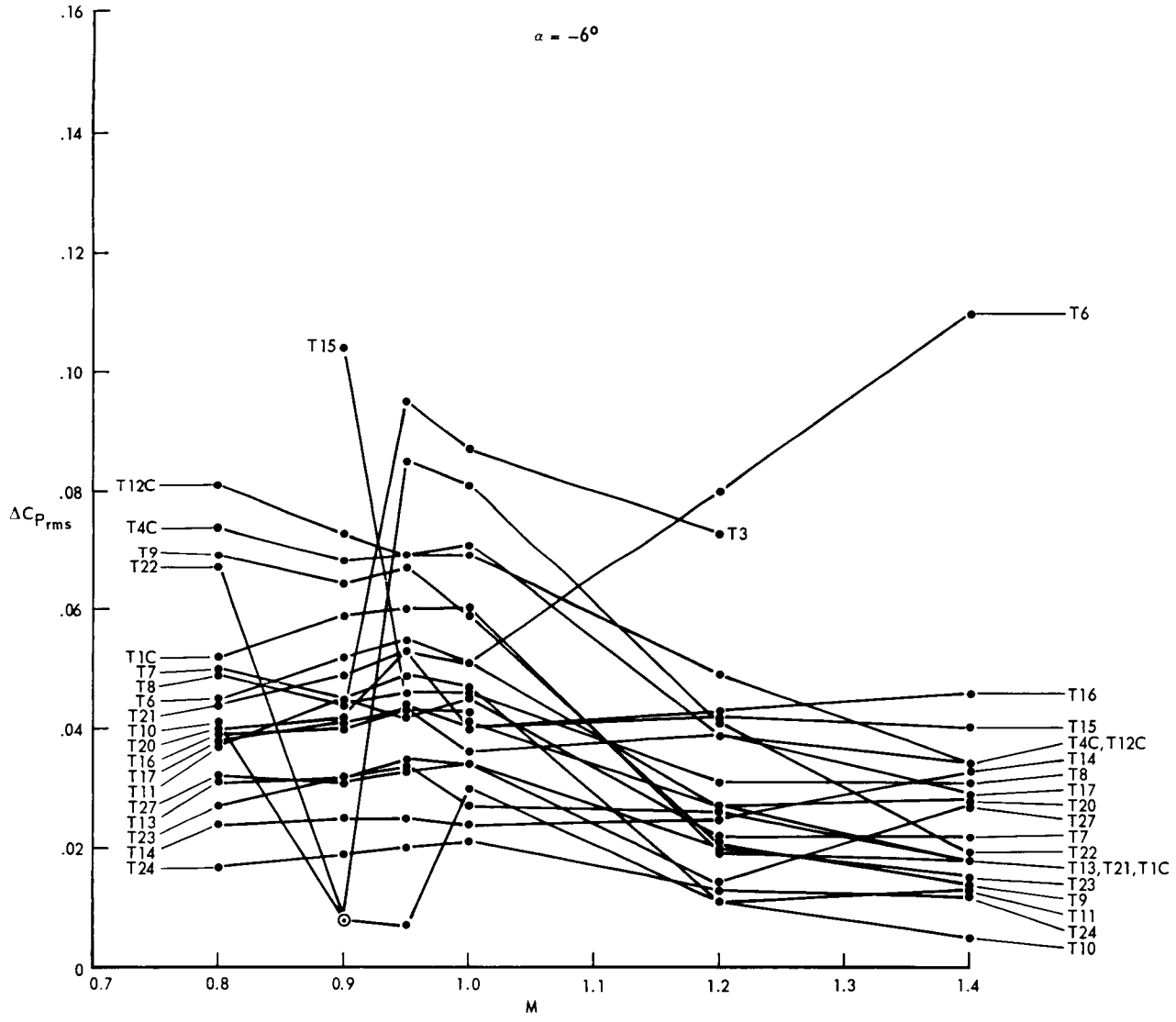

Figure 2 – Variation of Fluctuating Pressure Coefficients with Mach Number for Various Transducer Locations: MA–2 (Concluded)

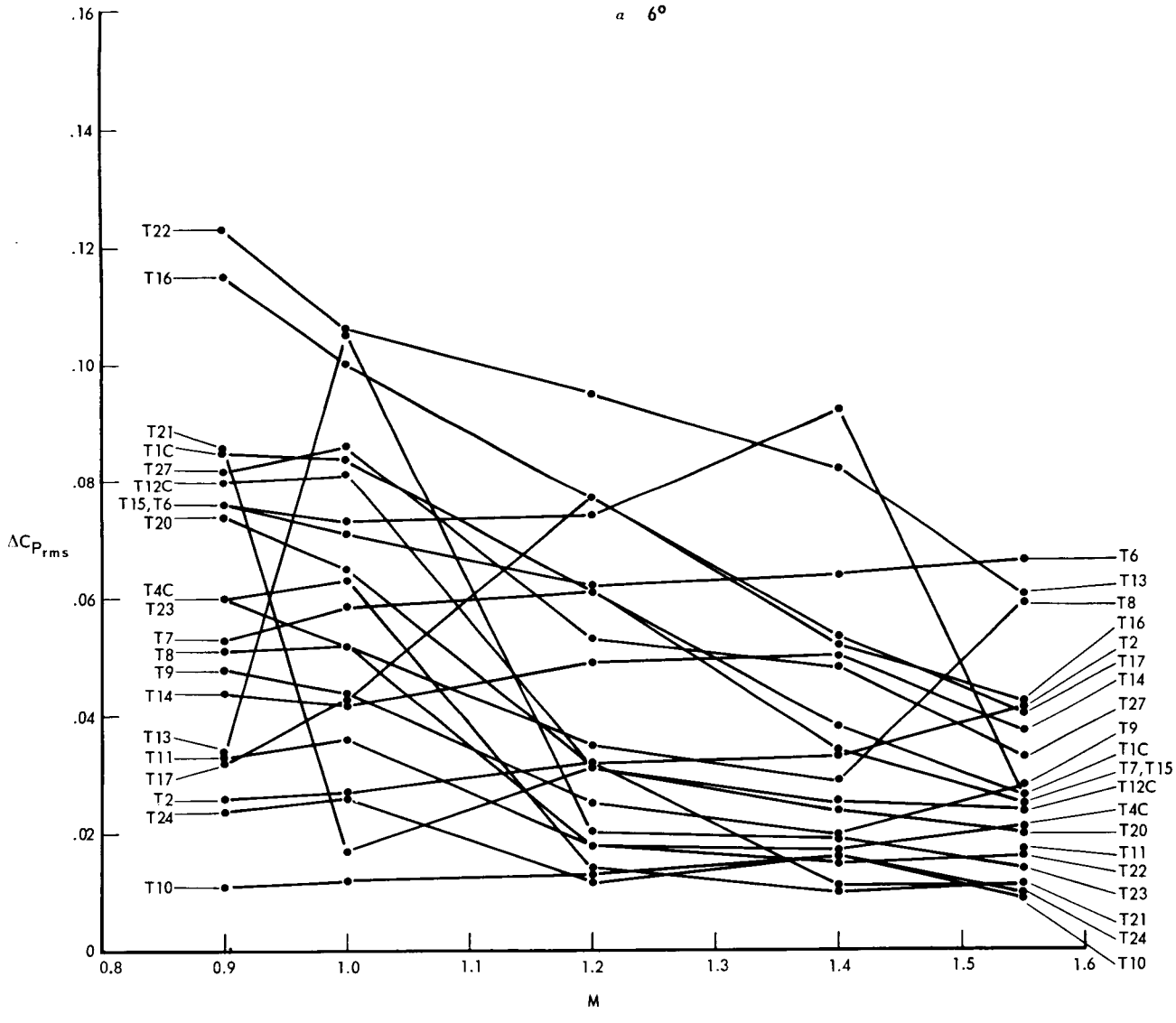

Figure 3 – Variation of Normalized Pressure Coefficient with Mach Number for Various Transducer Locations: MA–1

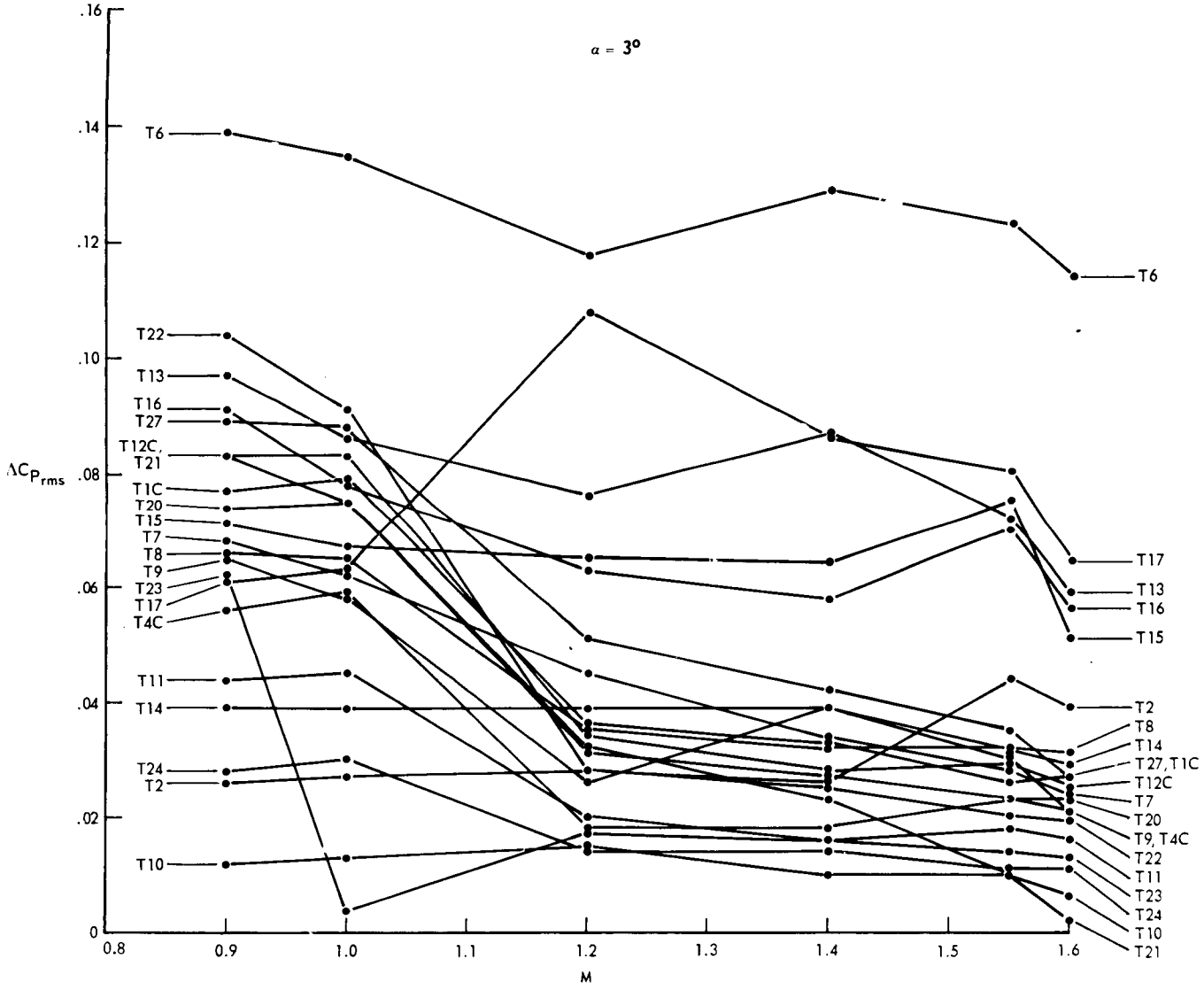

Figure 3 – Variation of Normalized Pressure Coefficient with Mach Number for Various Transducer Locations: MA–1 (Continued)

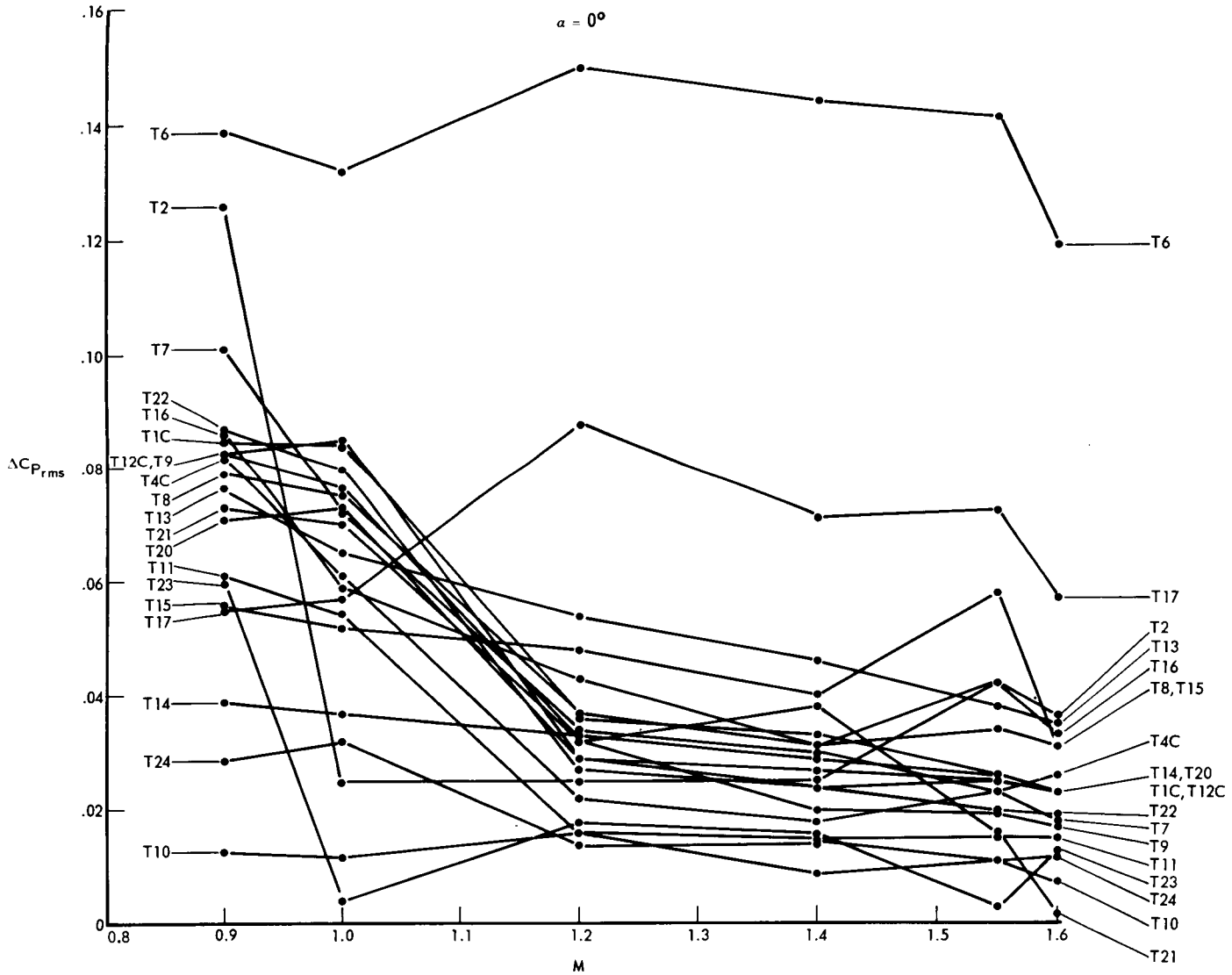

Figure 3 – Variation of Normalized Pressure Coefficient with Mach Number for Various Transducer Locations: MA–1 (Continued)

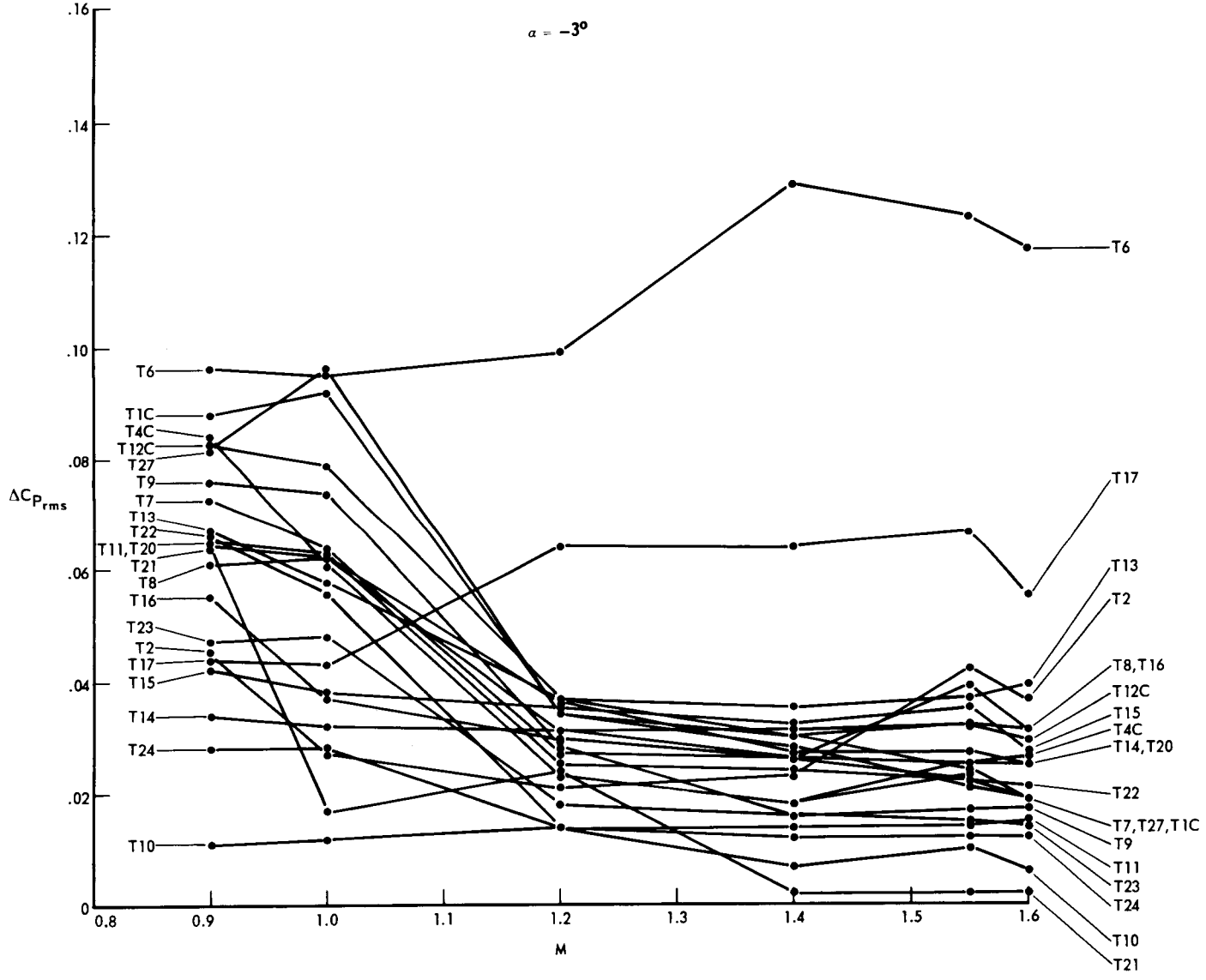

Figure 3 – Variation of Normalized Pressure Coefficient with Mach Number for Various Transducer Locations: MA–1 (Continued)

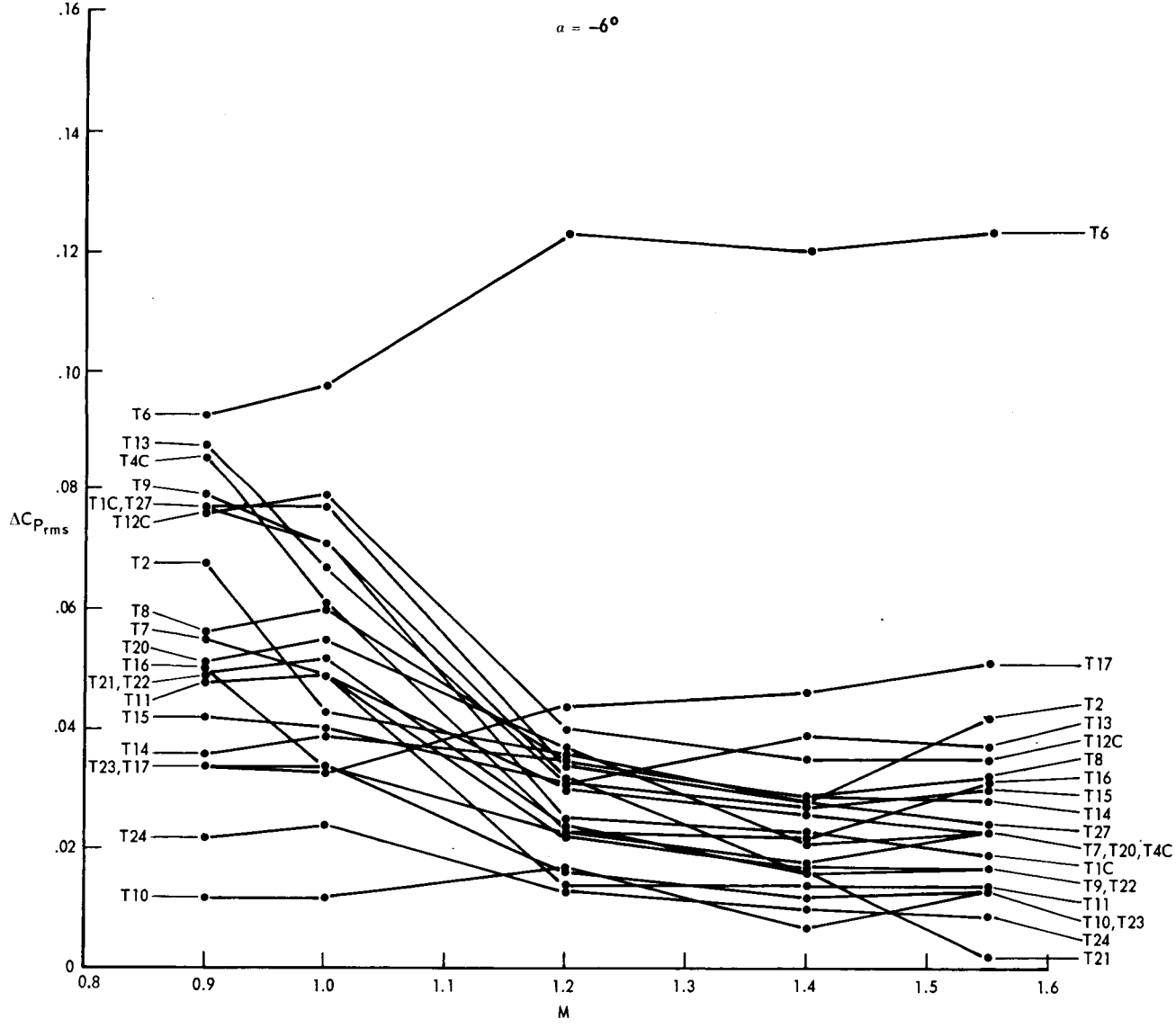

Figure 3 – Variation of Normalized Pressure Coefficient with Mach Number for Various Transducer Locations: MA–1 (Concluded)

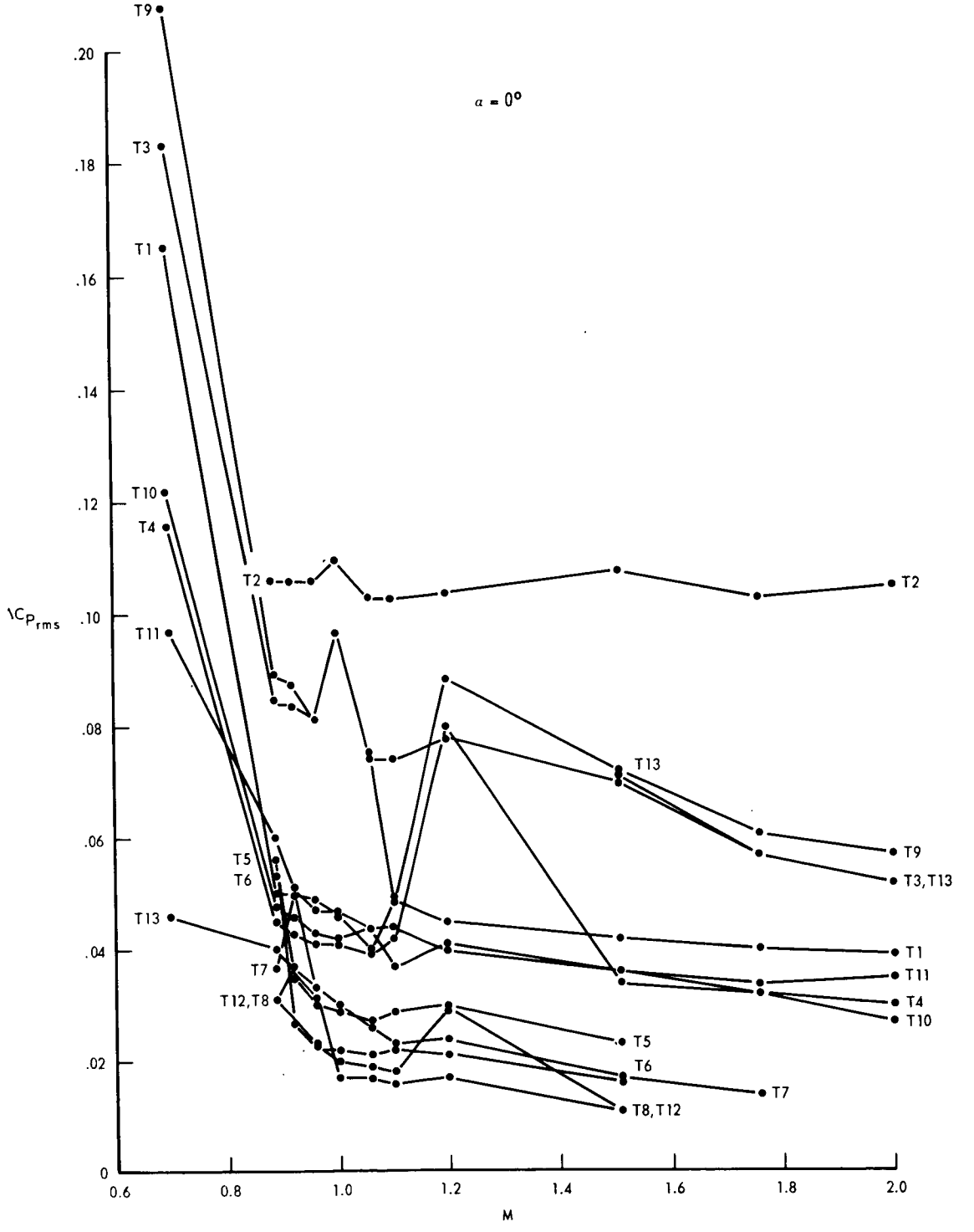

Figure 4 – Variation of Fluctuating Pressure Coefficient with Mach Number for Various Transducer Locations: AS–C

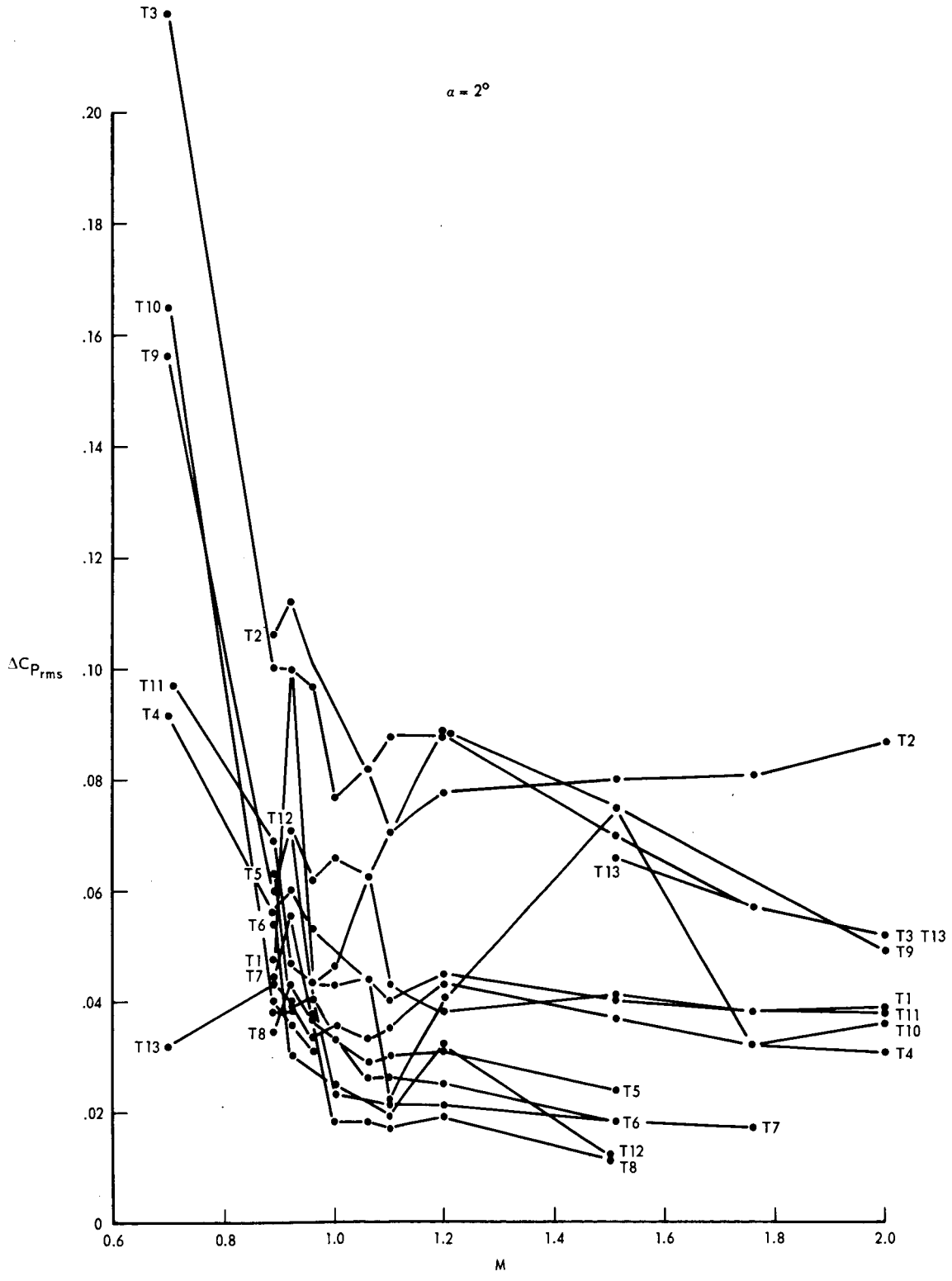

Figure 4 – Variation of Fluctuating Pressure Coefficient with Mach Number for Various Transducer Locations: AS–C (Continued)

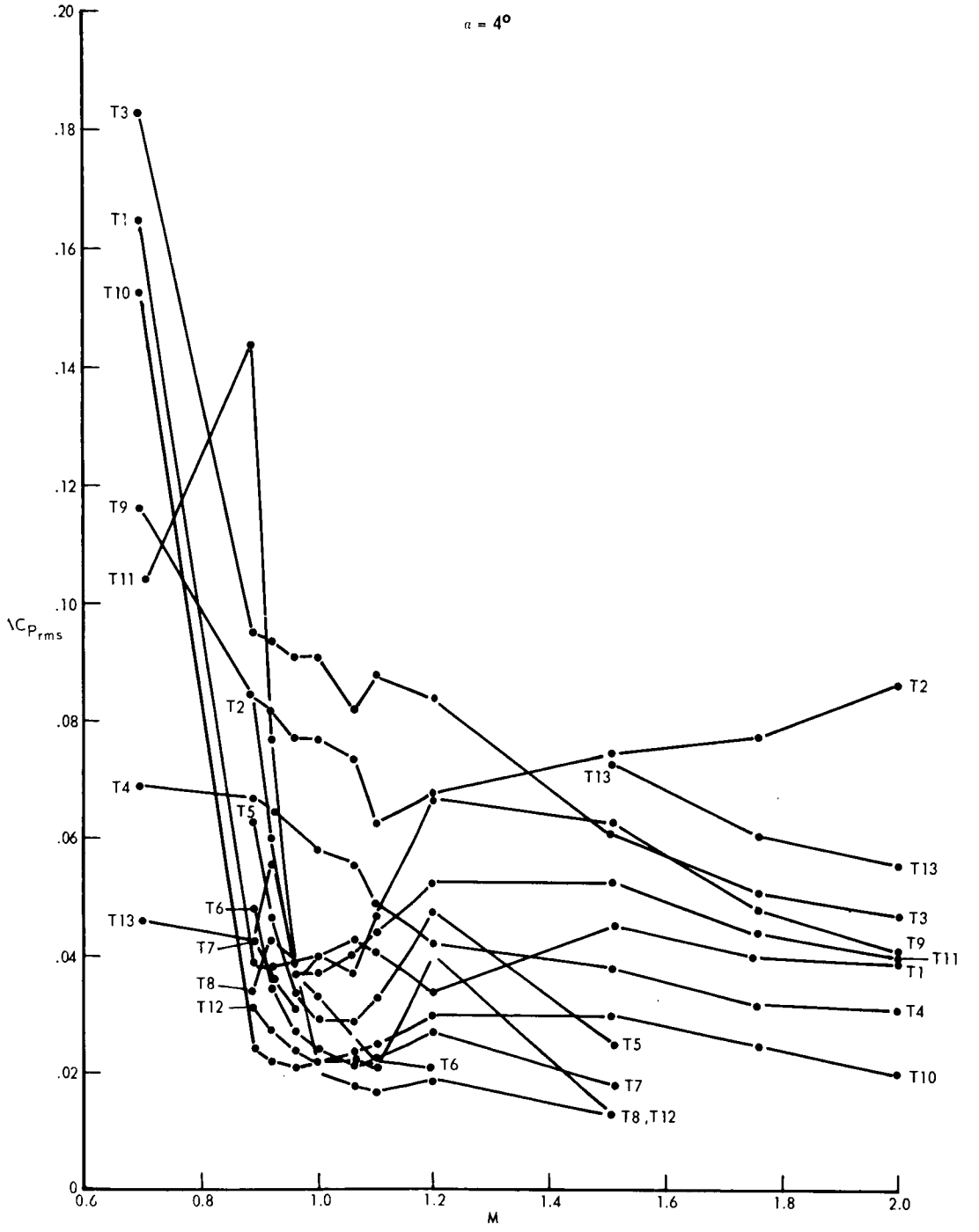

Figure 4 – Variation of Fluctuating Pressure Coefficient with Mach Number for Various Transducer Locations: AS–C (Continued)

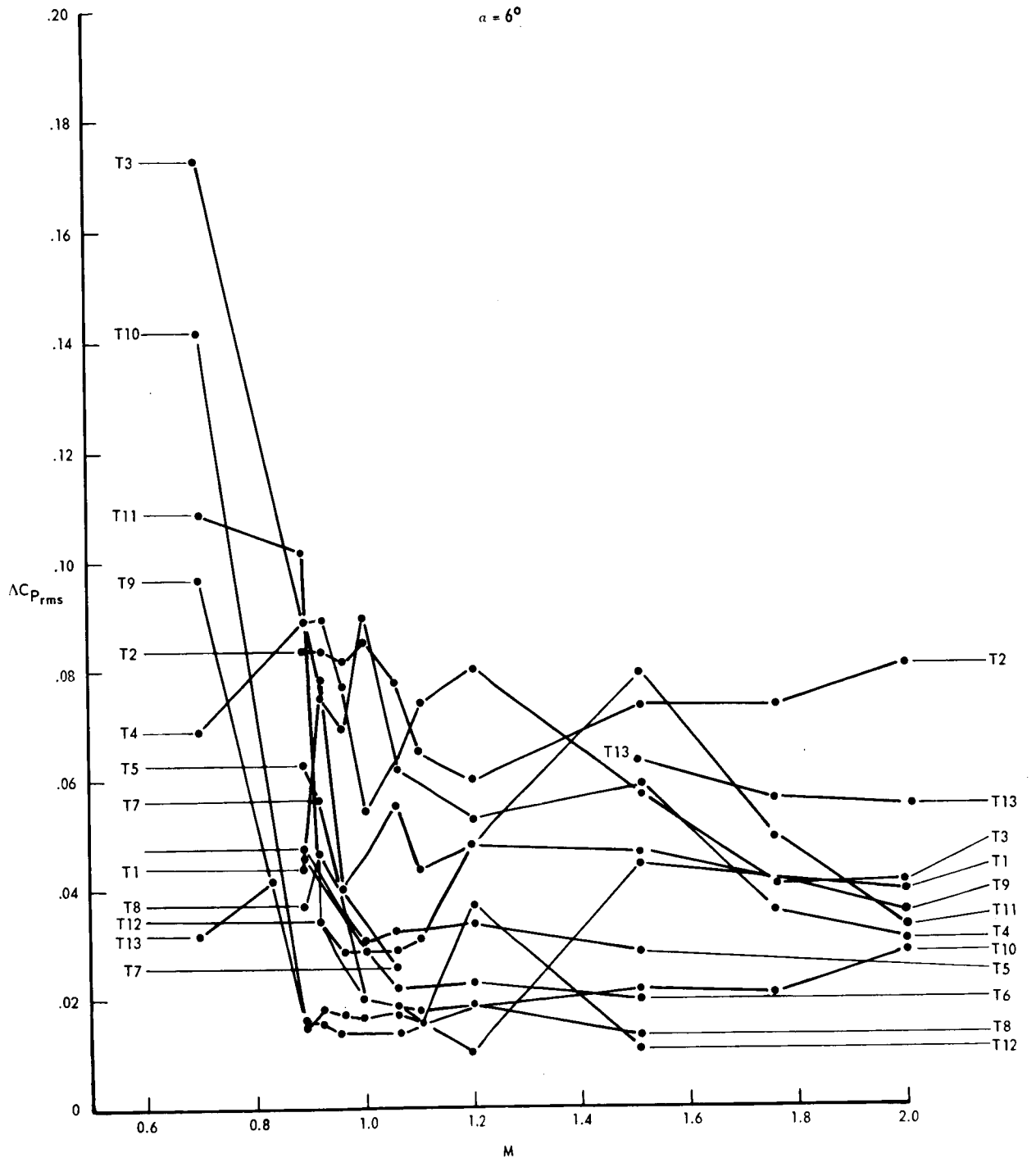

Figure 4 – Variation of Fluctuating Pressure Coefficient with Mach Number for Various Transducer Locations: AS–C (Concluded)

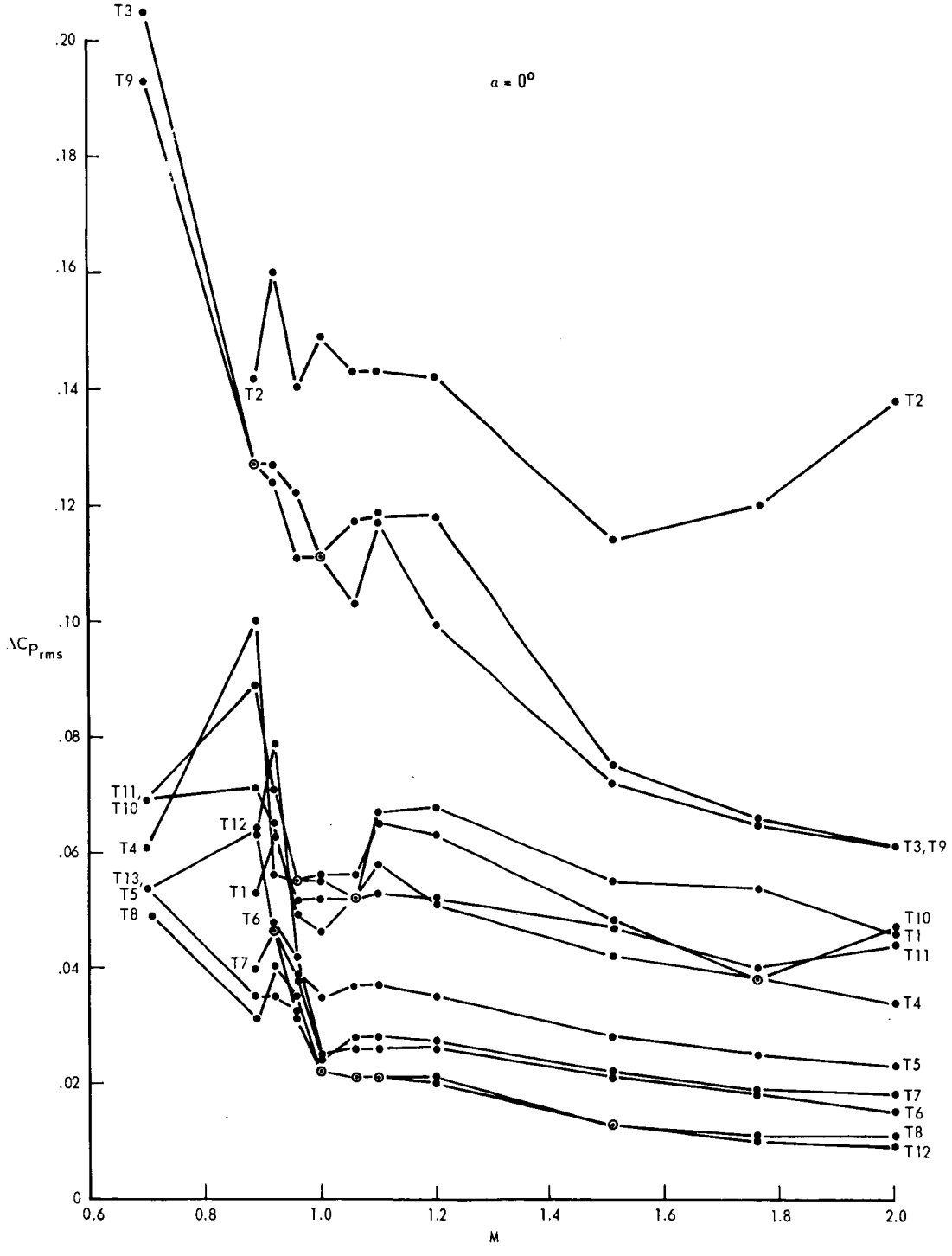

Figure 5 – Variation of Normalized Pressure Coefficients with Mach Number for Various Transducer Locations: AS–D

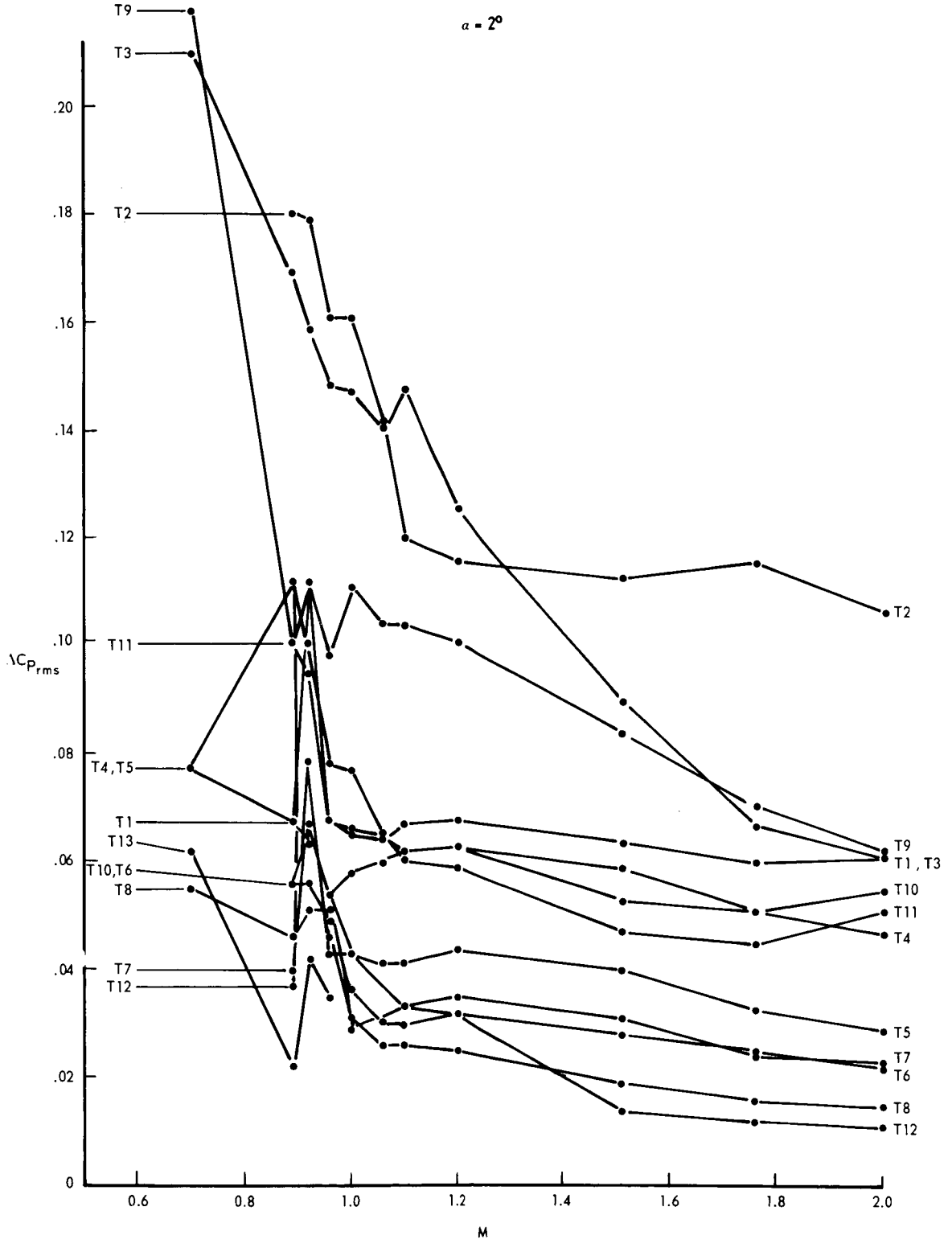

Figure 5 – Variation of Fluctuating Pressure Coefficients with Mach Number for Various Transducer Locations: AS-D (Continued)

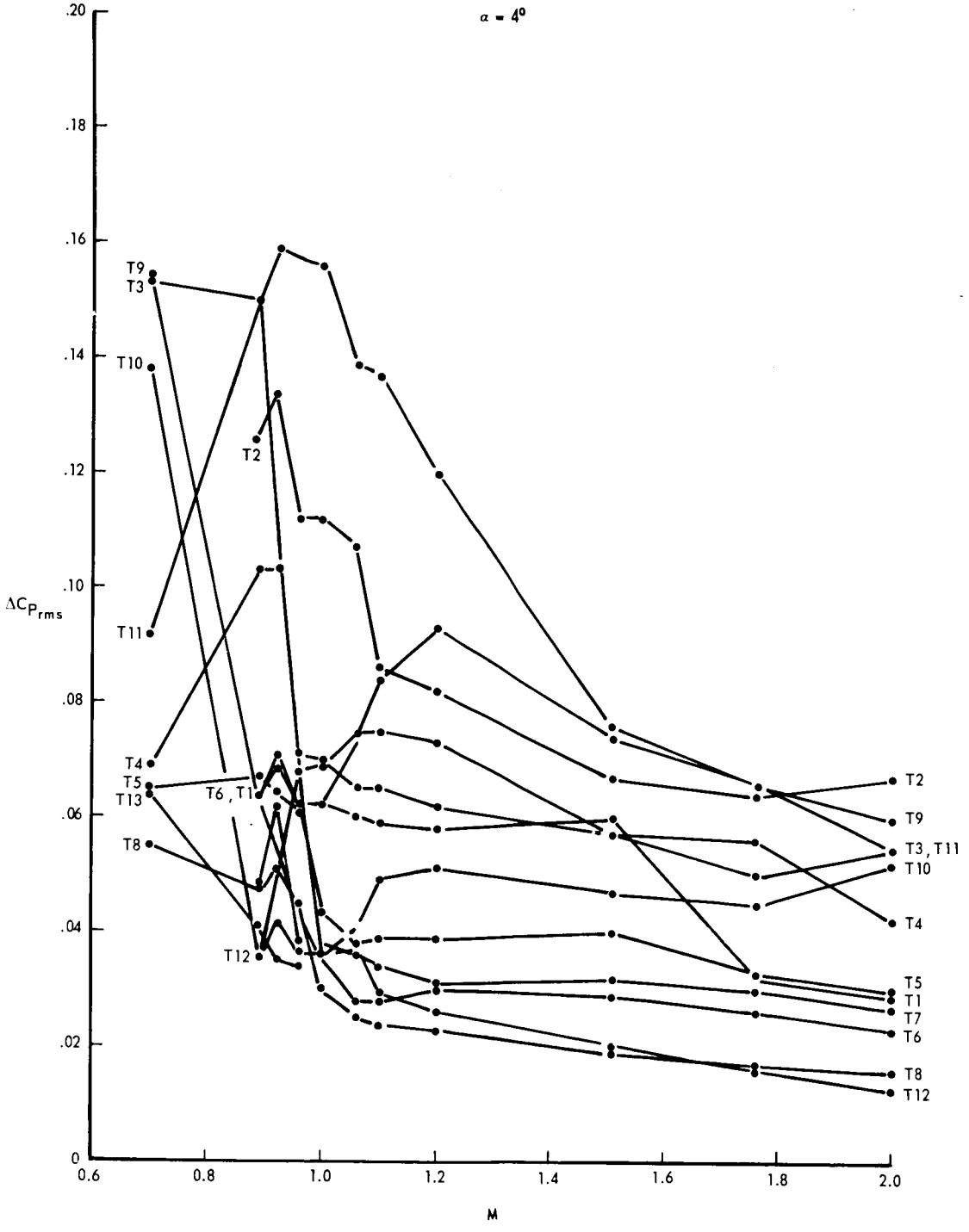

Figure 5 – Variation of Fluctuating Pressure Coefficients with Mach Number for Various Transducer Locations: AS–D (Continued)

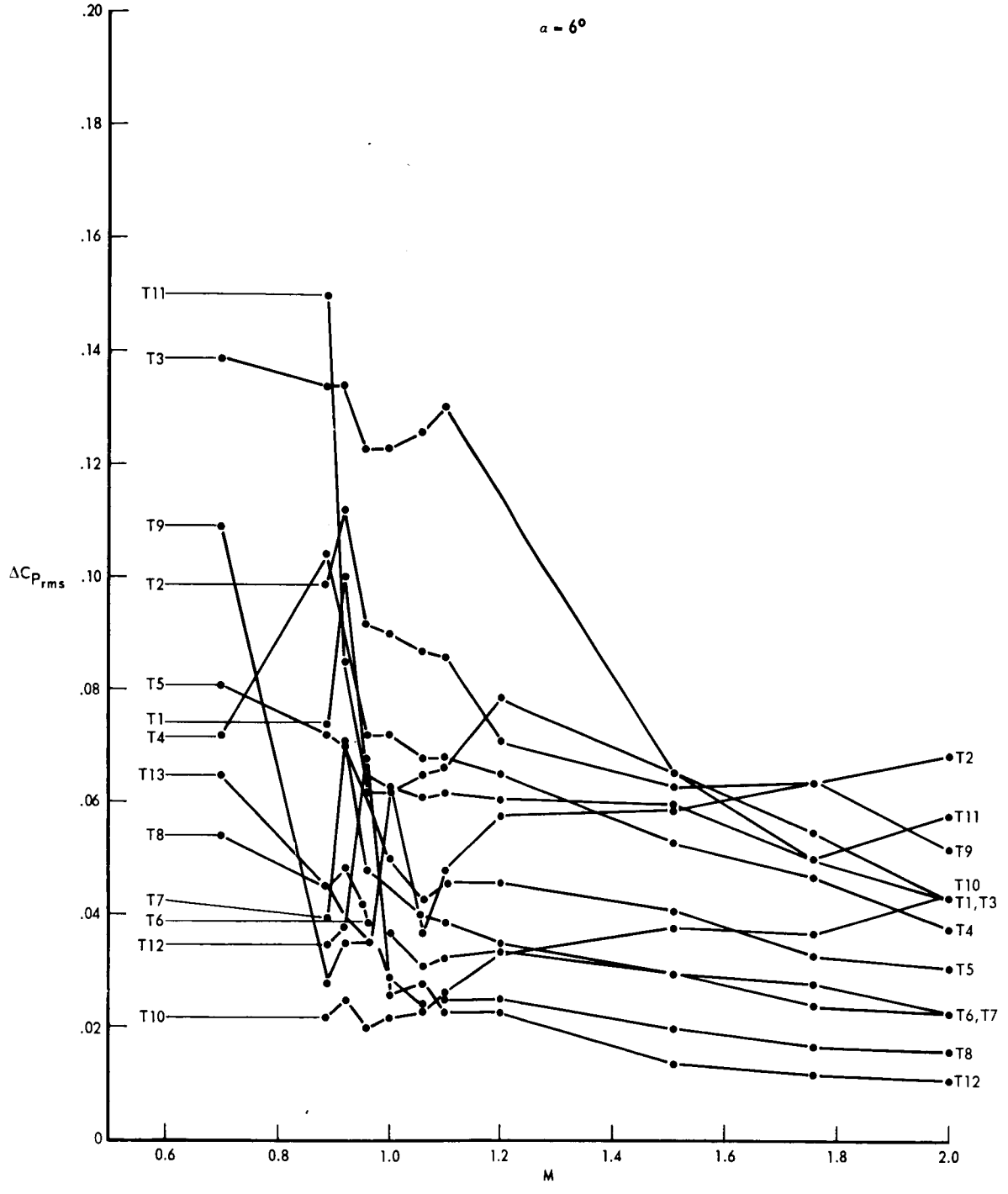

Figure 5 – Variation of Fluctuating Pressure Coefficients with Mach Number for Various Transducer Locations: AS–D (Concluded)

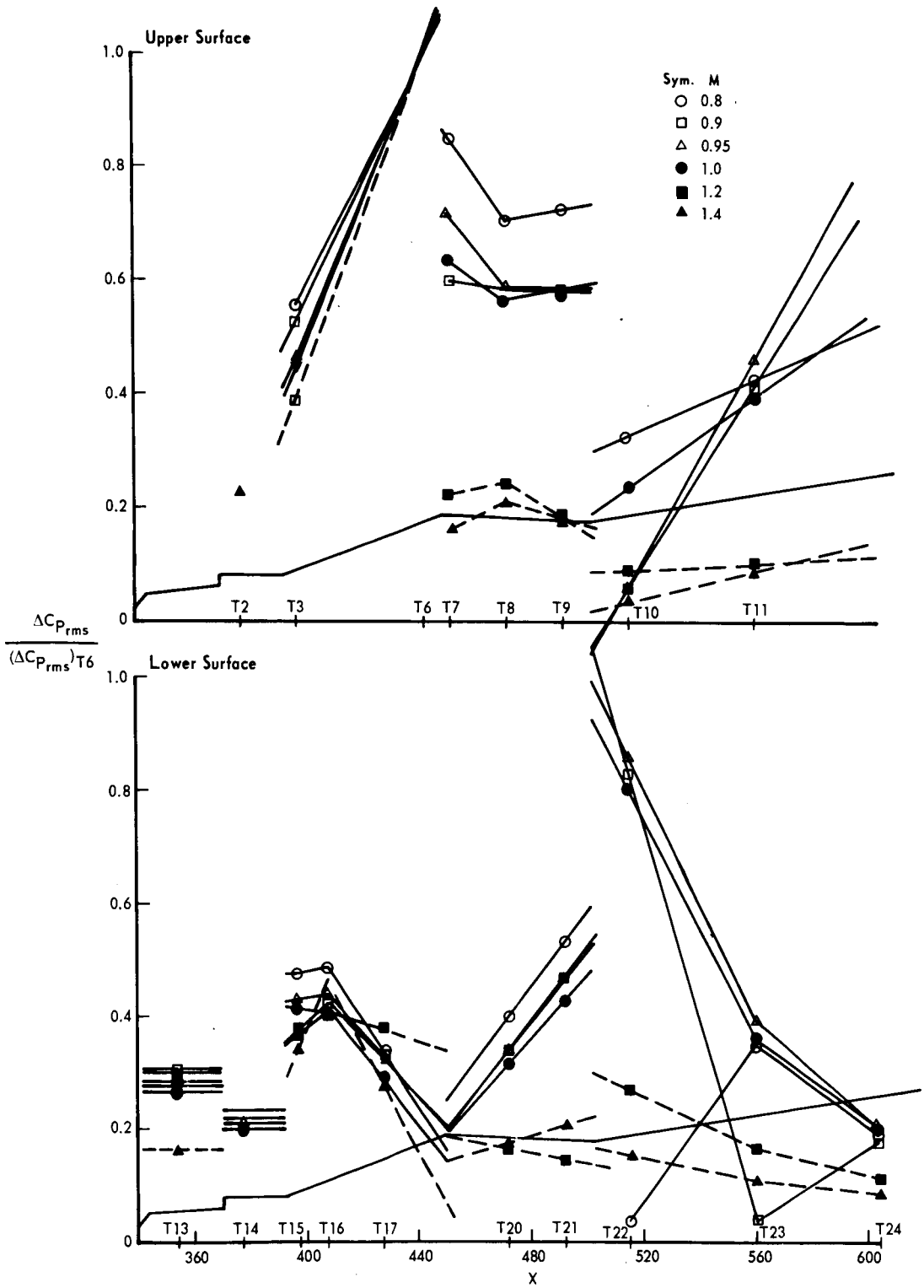

Figure 6 – Variation of Normalized Pressure Coefficient with Streamwise Location: MA–2, $\alpha = 0°$

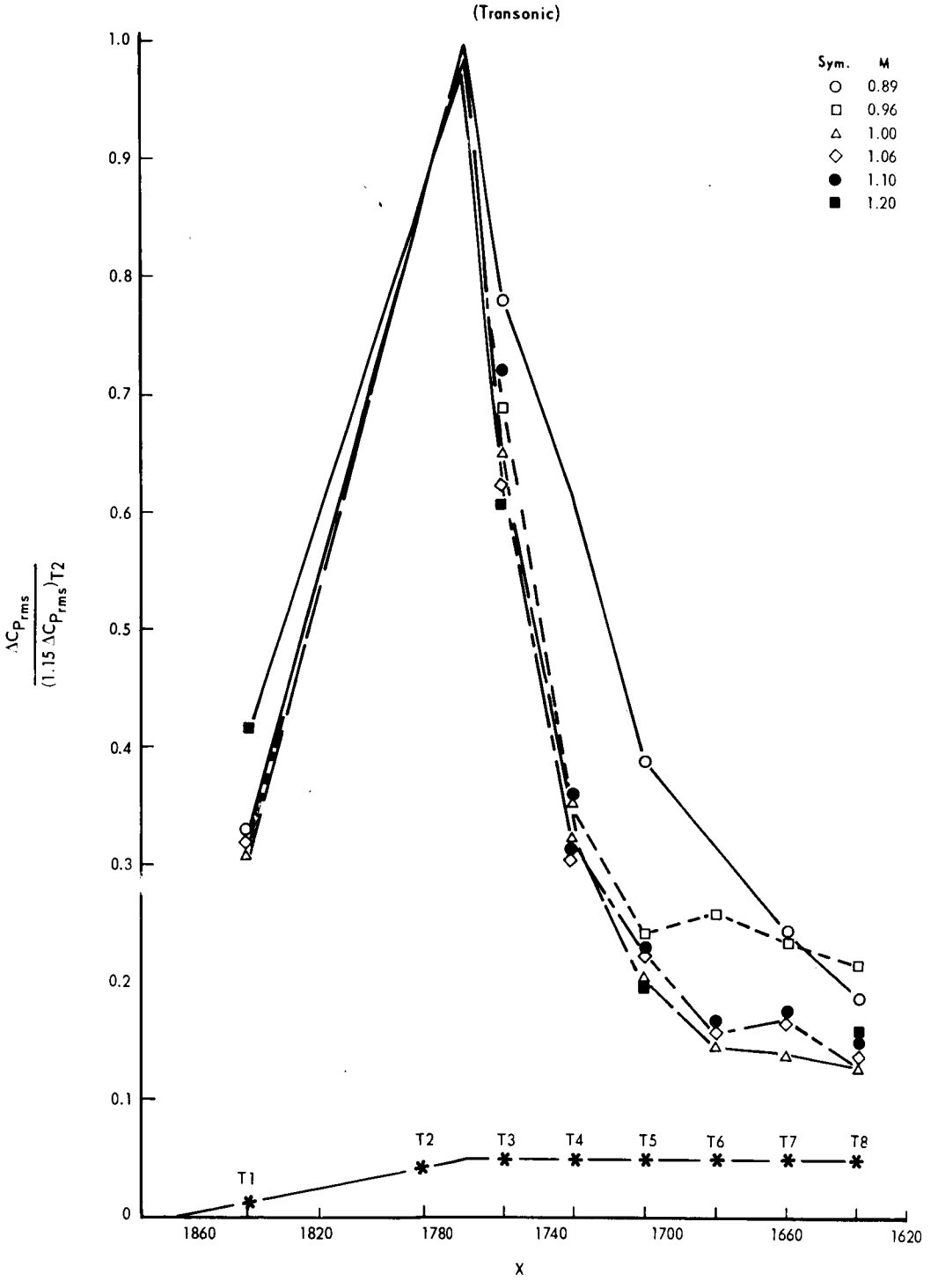

Figure 7 – Variation of Normalized Pressure Coefficients with Streamwise Location: AS–D, $\alpha = 0^{o}$

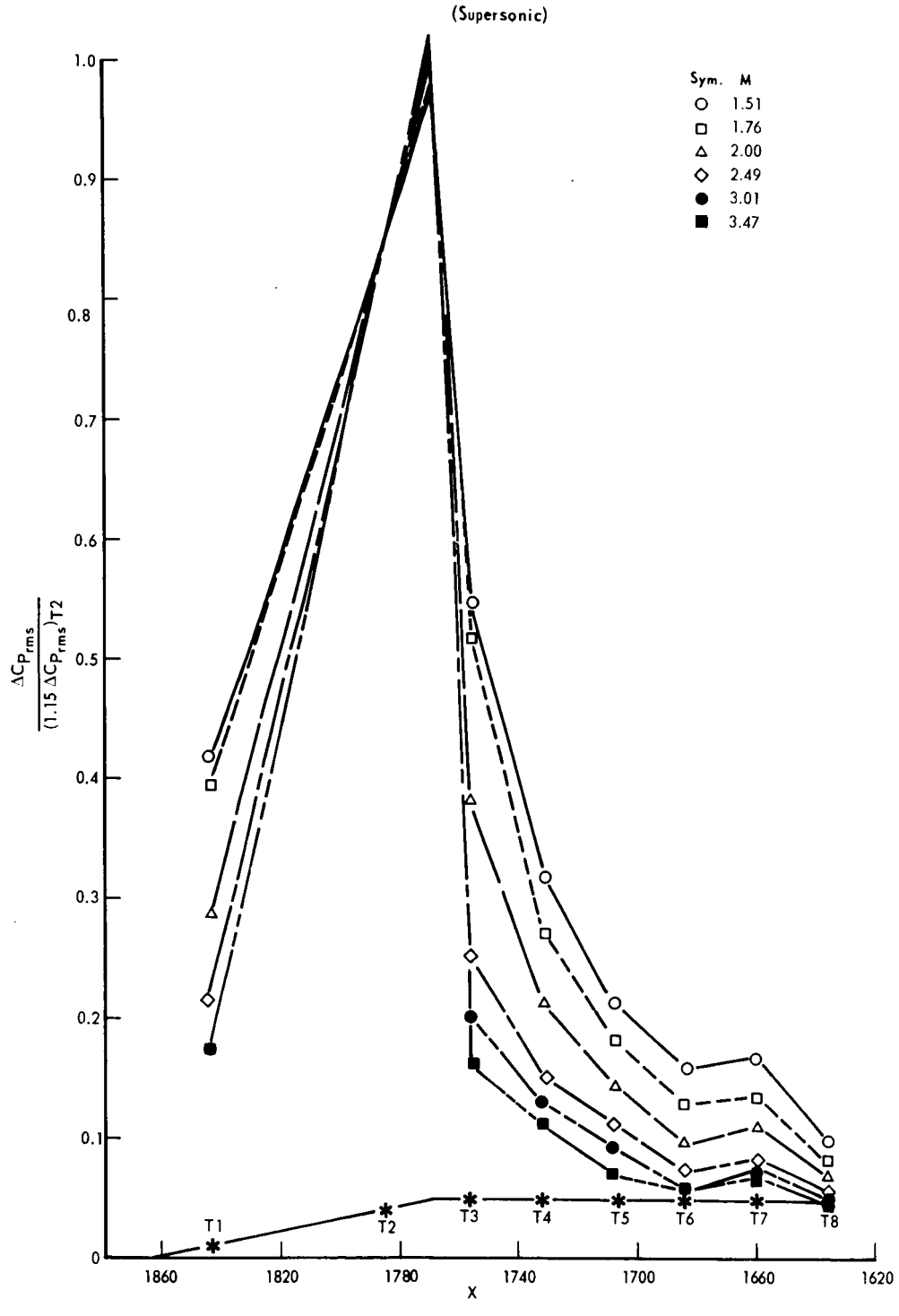

Figure 7 – Variation of Normalized Pressure Coefficients with Streamwise Location: AS–D, $\alpha = 0^{\circ}$ (Concluded)

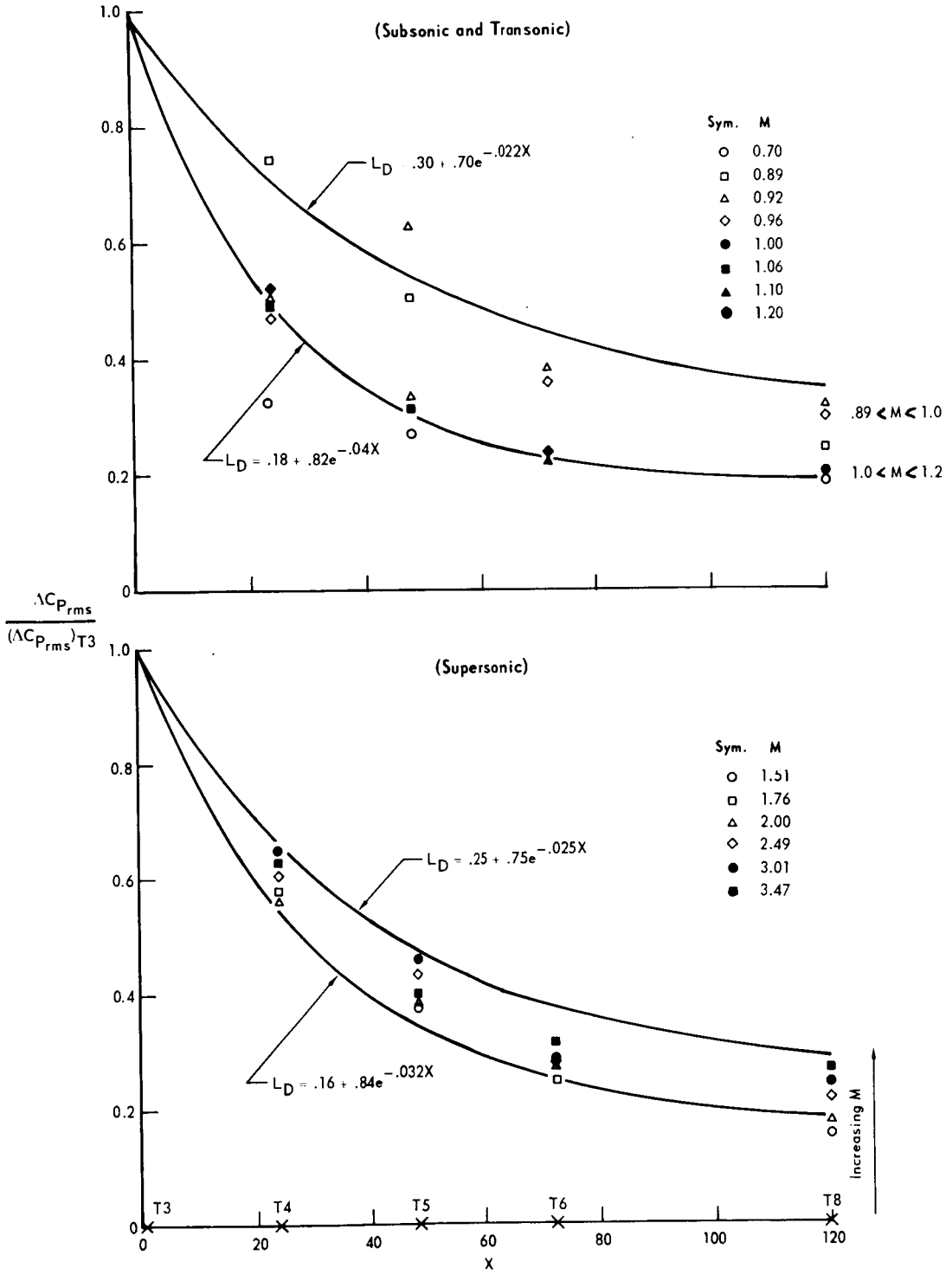

Figure 8 – Variation of Normalized Pressure Coefficients with Streamwise Location: AS–D, $\alpha = 0^o$

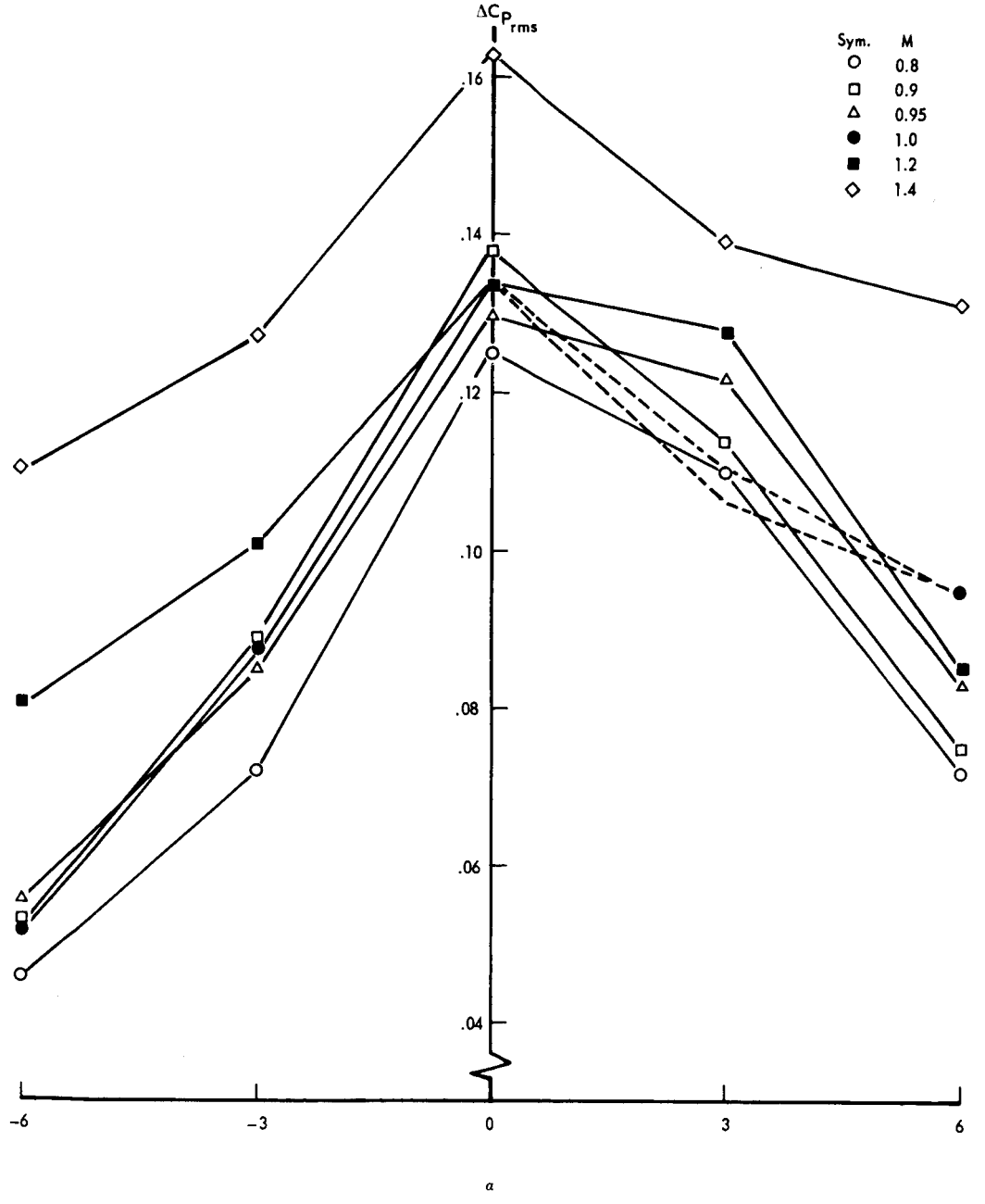

Figure 9 – Variation of Fluctuating Pressure Coefficient at Transducer 6 with Angle of Attack: MA-2

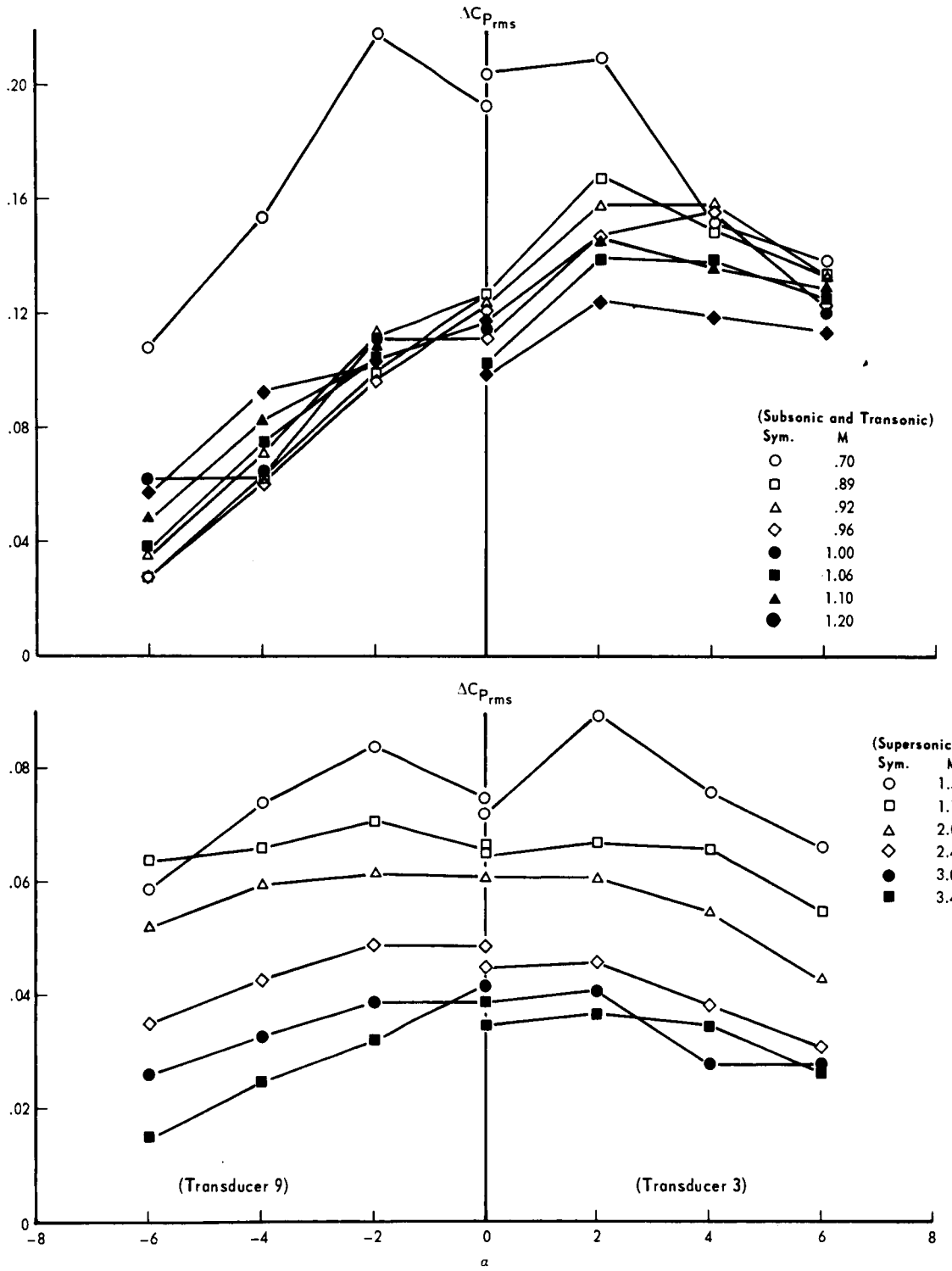

Figure 10 – Variation of Fluctuating Pressure Coefficient with Angle of Attack: AS–D

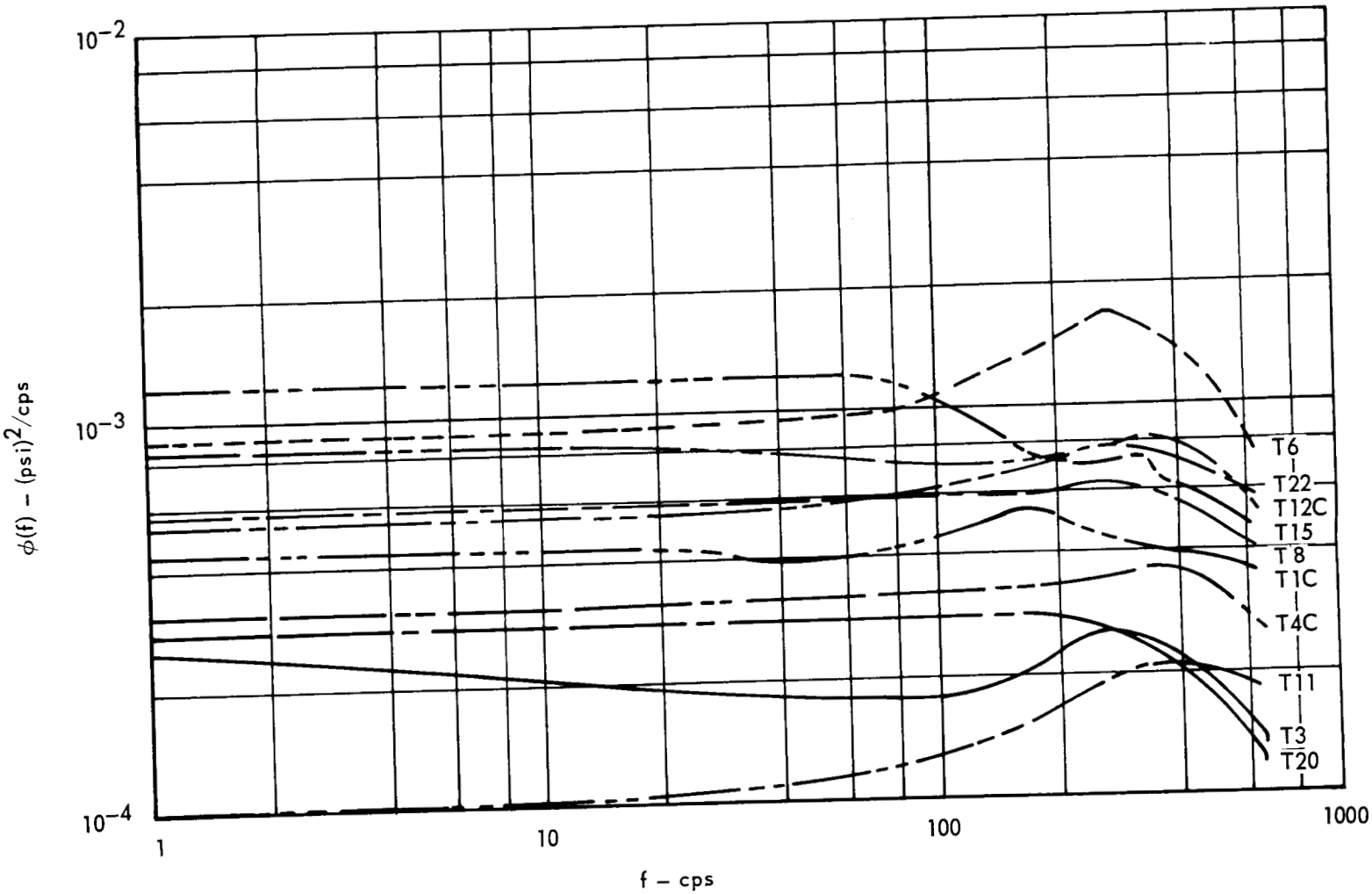

Figure 11 – Power Spectral Density of Fluctuating Buffet Pressure: MA–2, M = 1.0, $\alpha = 3^o$

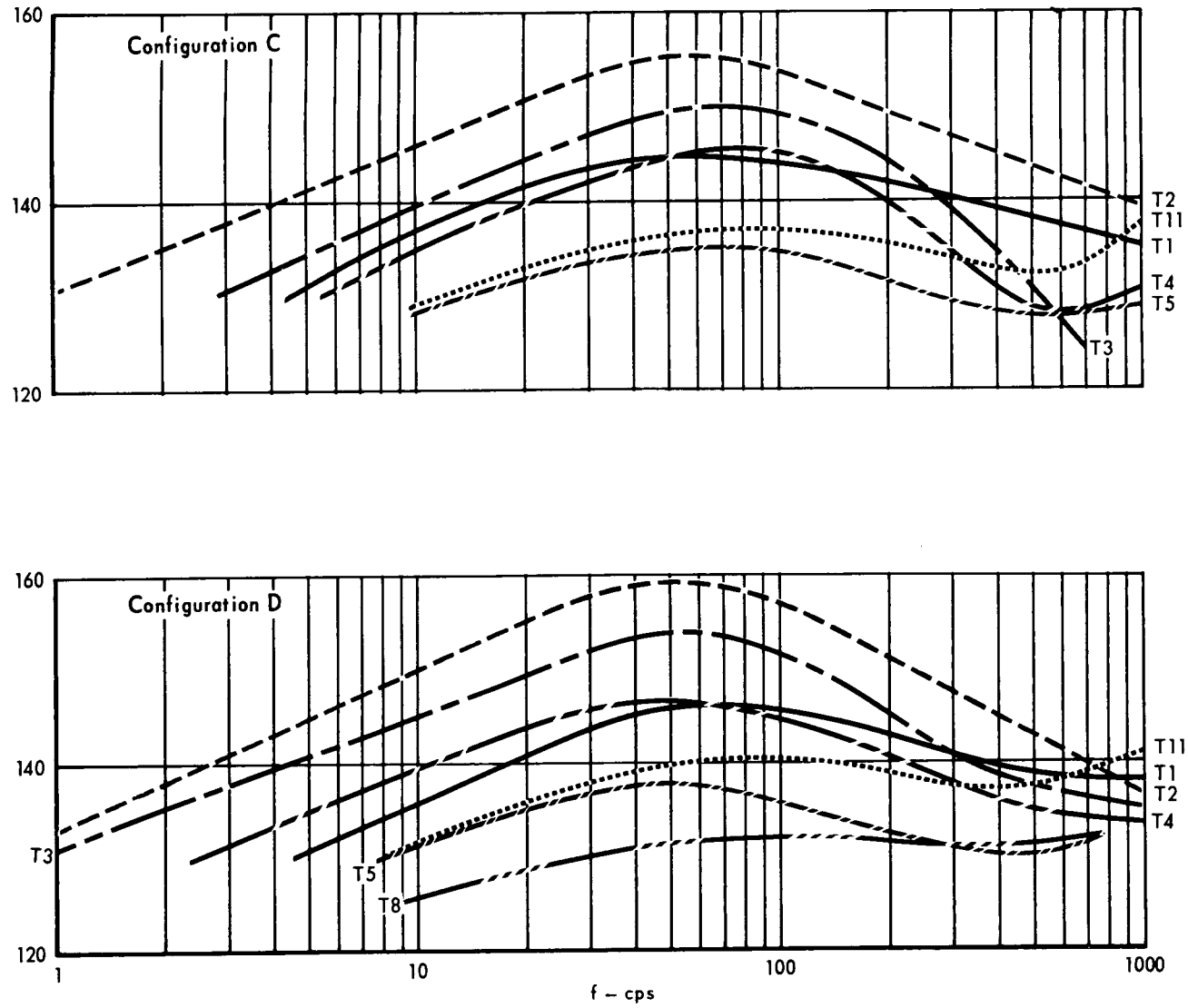

Figure 12 – Frequency Spectra of Apollo Sound Pressure Levels: M = 1.0, $\alpha = 0^{o}$

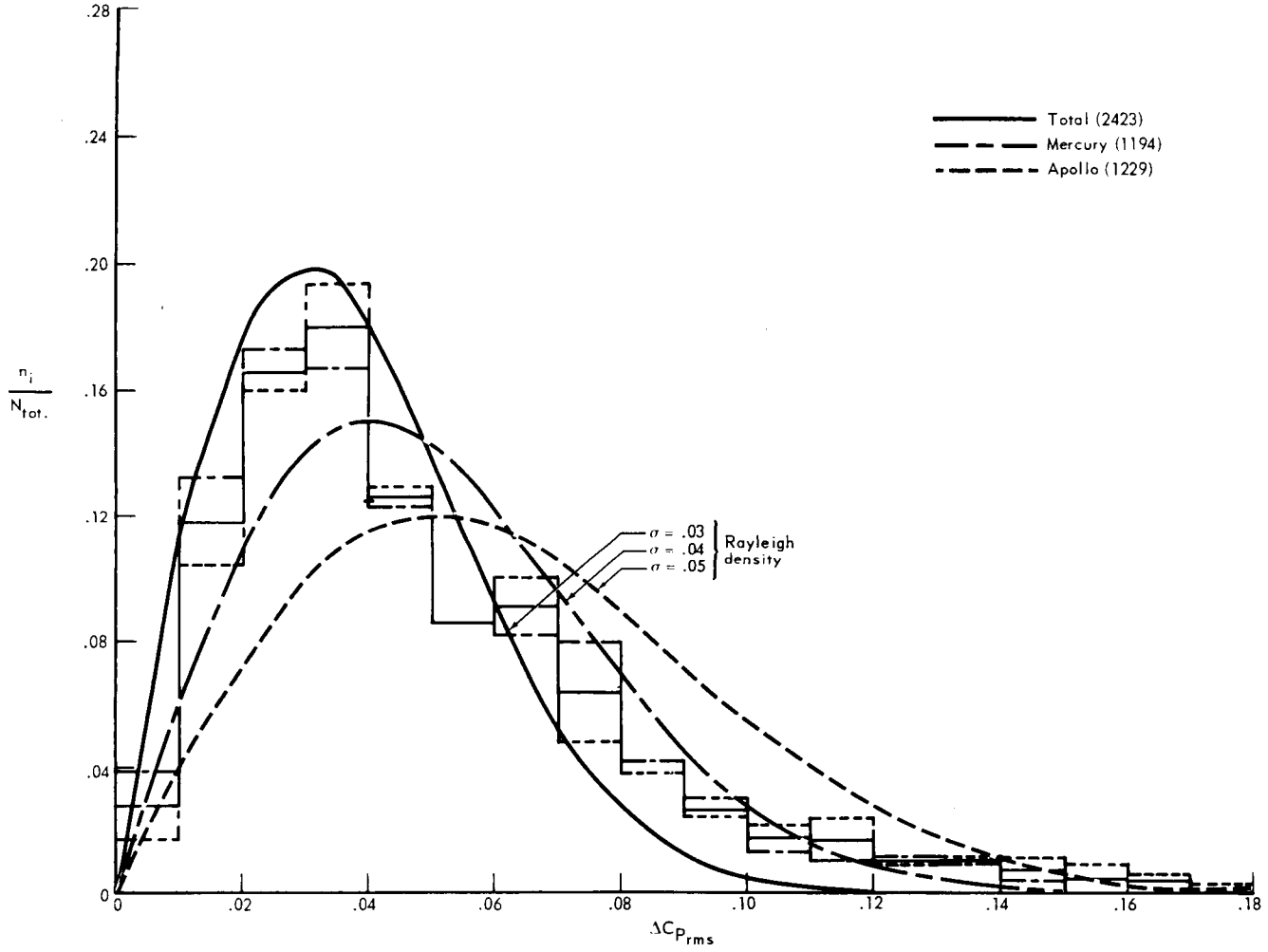

Figure 13 – Density Distribution of Fluctuating Buffet Pressures for the Combined Mercury and Apollo Data and Separately for Mercury and Apollo

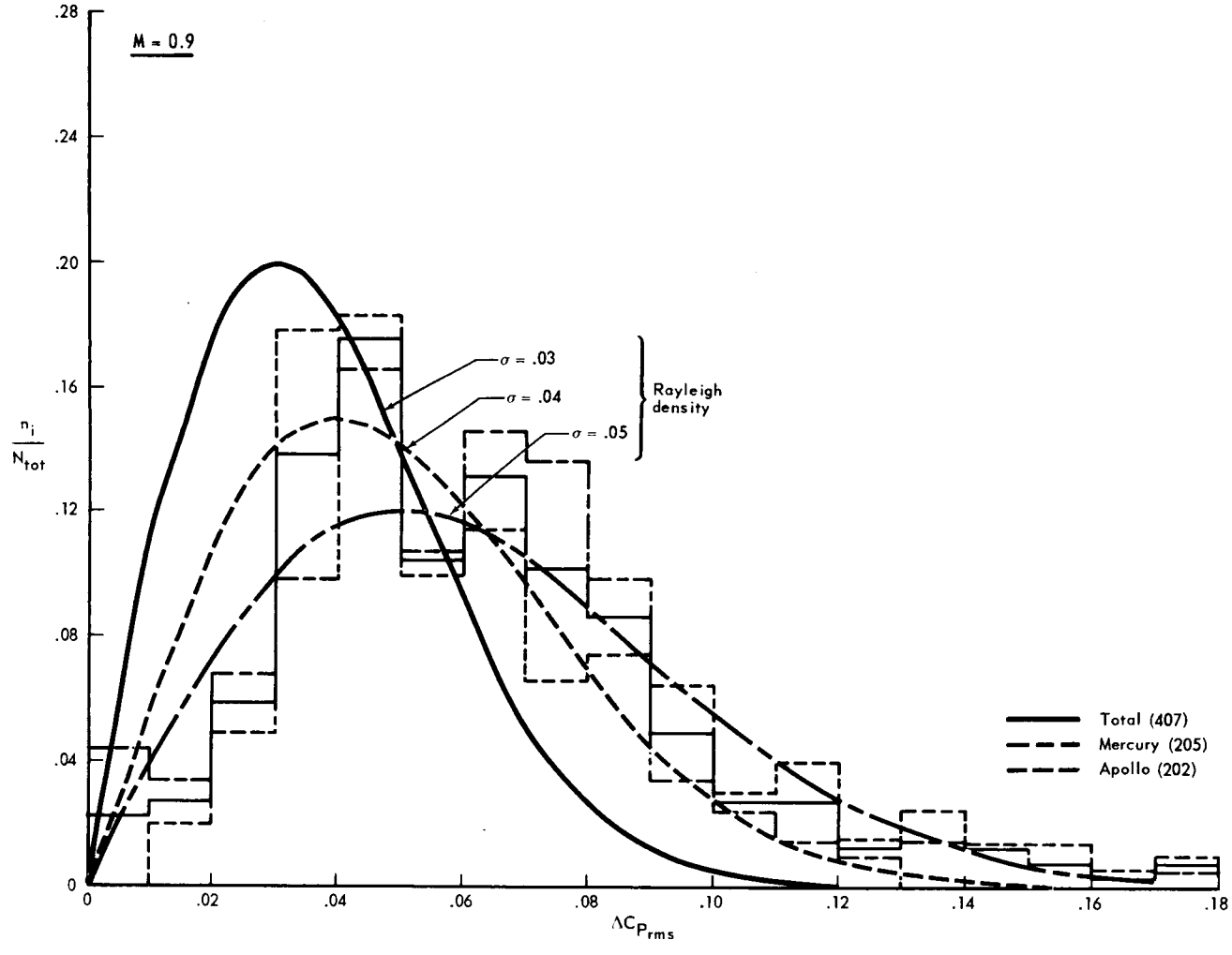

Figure 14 – Density Distribution of Fluctuating Buffet Pressures at Three Mach Numbers

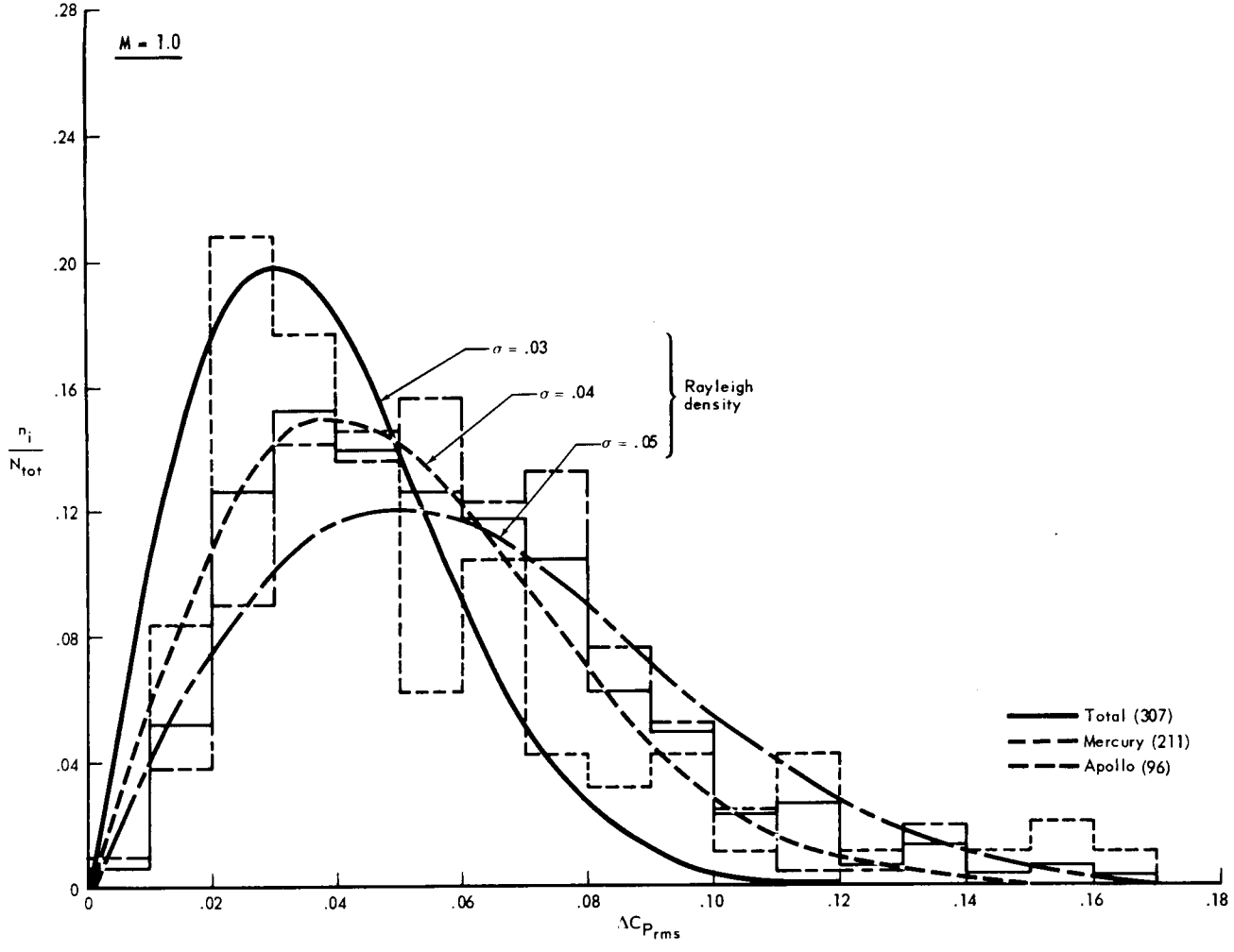

Figure 14 – Density Distribution of Fluctuating Buffet Pressures at Three Mach Numbers (Continued)

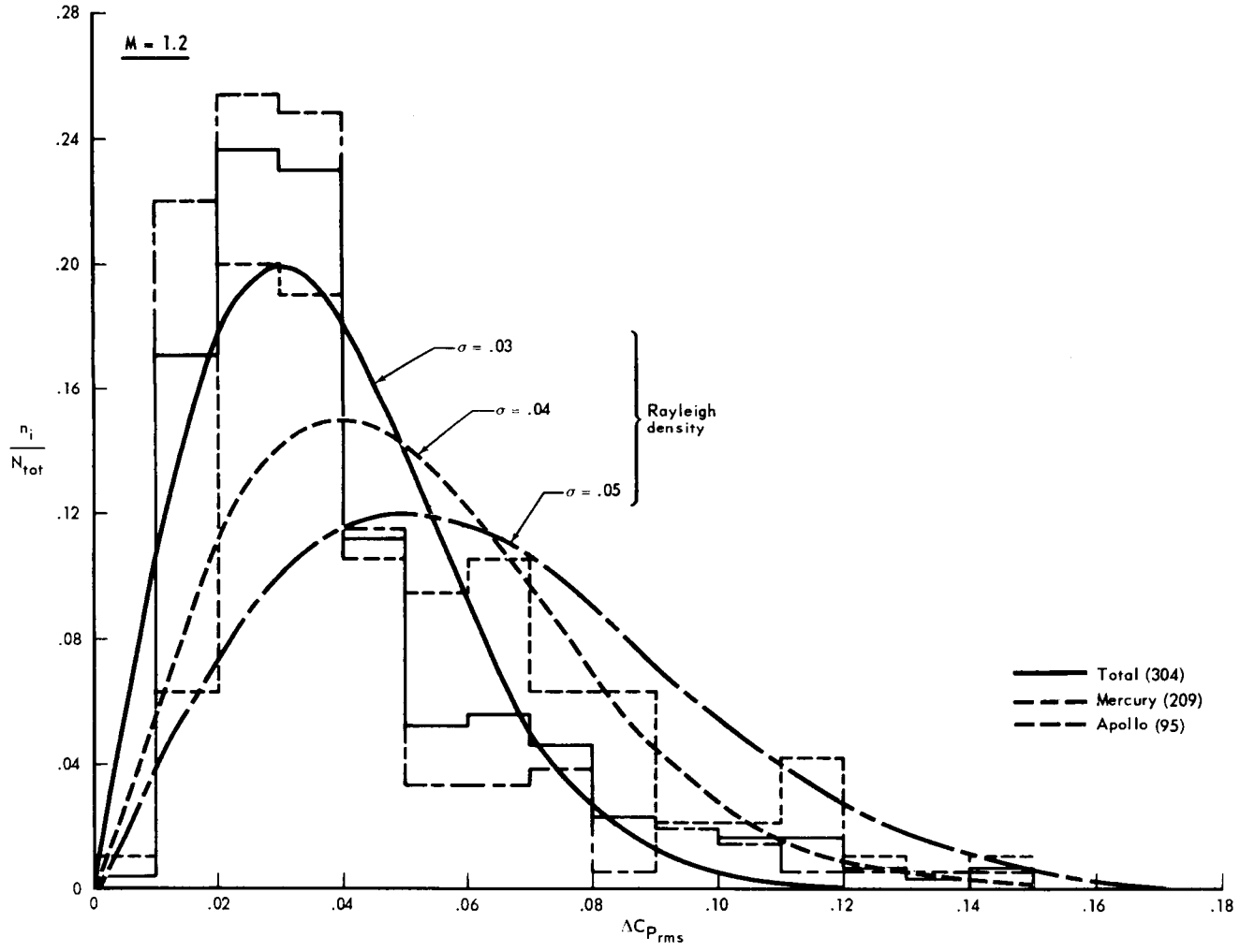

Figure 14 – Density Distribution of Fluctuating Buffet Pressures at Three Mach Numbers (Concluded)

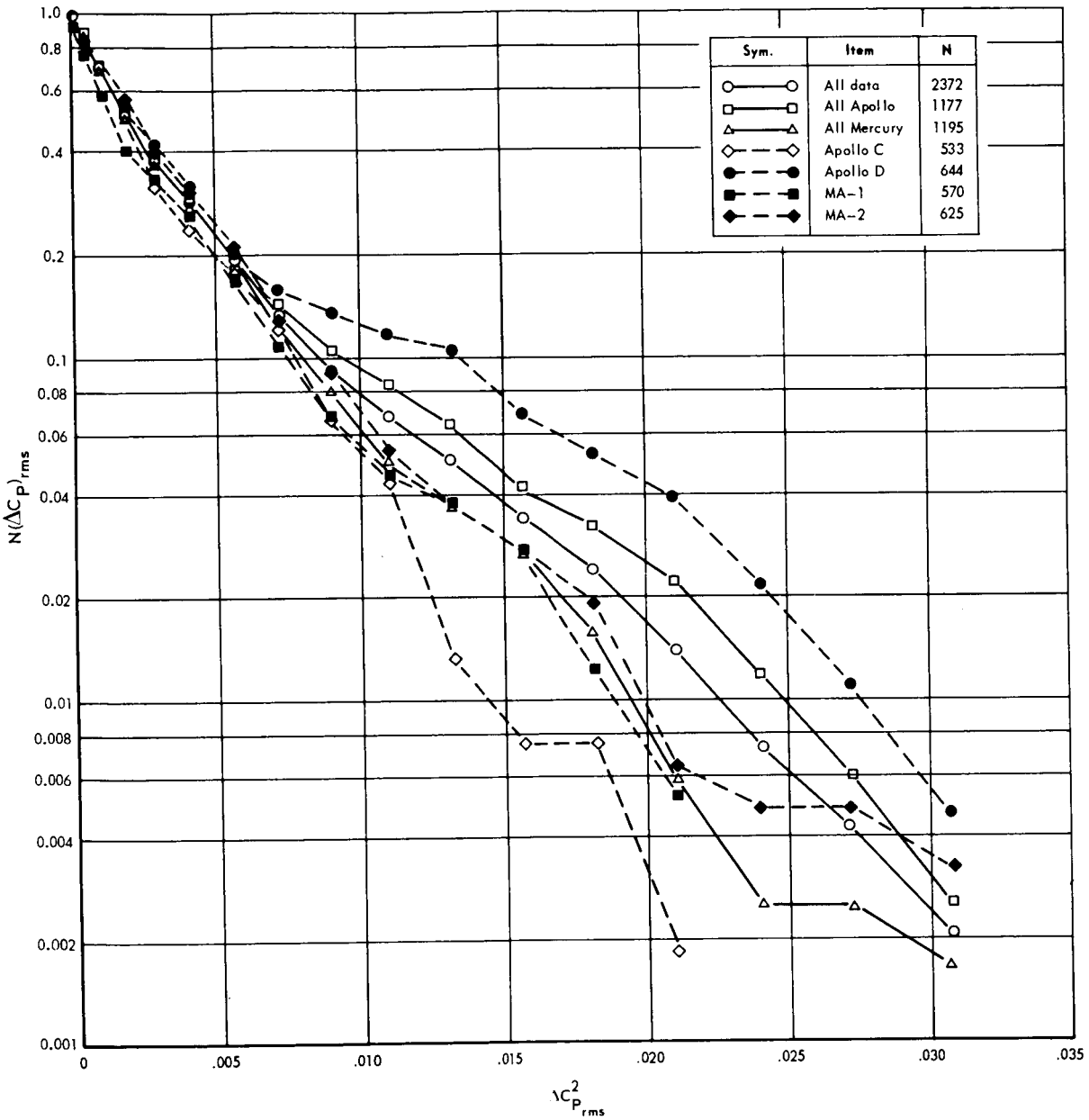

Figure 15 – Combined Probability Distribution of Fluctuating Buffet Pressures